Material Matters™

Volume 7, Number 1

ALDRICH Materials Science

Innovative Materials for High-Performance Optoelectronic Devices

OPVs, OFETs, and OLEDs

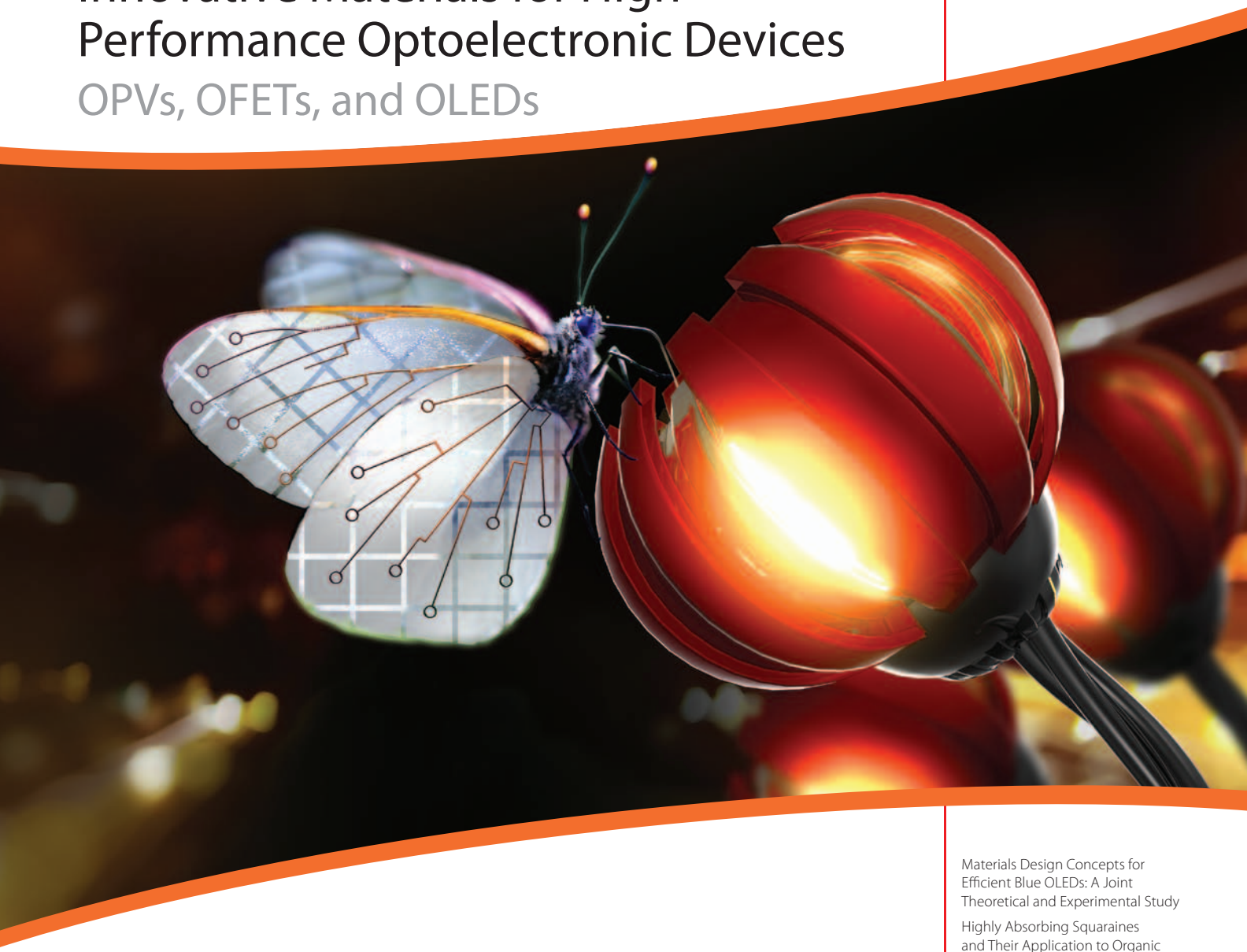

Materials for Illuminating Technology

Introduction

Yong Zhang, Ph.D.
Aldrich Materials Science
Sigma-Aldrich Co. LLC

Welcome to the first issue of *Material Matters*™ for **2012**, focused on high-performance organic optoelectronic devices. Since their discovery, devices such as organic light-emitting diodes (OLEDs), organic photovoltaic solar cells (OPVs), and organic field effect transistors (OFETs) have triggered enormous scientific interest, as well as skepticism regarding their potential for commercial application. As of today, there are several notable examples that have made their high-performance future much brighter: organic solar cells based on conjugated polymers and fullerene derivatives blends have achieved nearly a 10-fold improvement of power conversion efficiency as compared to a decade ago; optimized OLEDs are approaching their theoretical limit in internal quantum efficiency; OFETs comprised of conjugated polymers have demonstrated carrier mobilities competitive with amorphous silicon. Moreover, OLEDs are now integrated in commercial display and lighting products. Researchers continue to make significant advances in materials chemistry and device engineering of organic semiconductors that will further the potential for commercial success of OLED, OFET, and OPV devices.

In this issue, we discuss a variety of innovative materials, including both organic/polymeric molecules and inorganic nanomaterials, which have made superior optoelectronic devices become reality. In the first article, Asanga B. Padmaperuma and Evgueni Polikarpov (Applied Materials Group, Pacific Northwest National Laboratory) describe a process to design functional OLED materials by correlating theoretical predictions and experimental measurements. This approach enables researchers to identify novel host and charge carrier materials with predicted electronic properties for optimized OLED performance. In the next article, Professor Thuc-Quyen Nguyen (University of California, Santa Barbara) illustrates her group's recent developments in conjugated small molecules containing a series of diketopyrrolopyrrole (DPP)-based chromophores for the fabrication of optoelectronic devices. They demonstrate the benefit of small molecules over their polymeric counterparts in terms of precise control over material properties. In the following article, Professor Alejandro L. Briseño and his group at the University of Massachusetts, Amherst summarize the synthetic history of thiophene-based materials for organic electronics and emphasize the importance of new processing techniques to increase crystallinity, which further improves device performance. Finally, Benny Pacheco and Scott Kordyban (Cytodiagnostics, Inc.) highlight some of the many recent advances in optoelectronics with well-defined inorganic nanomaterials. They emphasize that the key to enhanced performance is the use of precisely controlled nanomaterials.

Each article in this issue is accompanied by the corresponding Aldrich® Materials Science products which will facilitate research efforts in high-performance optoelectronic devices. For a comprehensive library of products and associated technical information, visit us at **Aldrich.com/matsci.** We welcome your comments, questions, new product suggestions and custom requests: **matsci@sial.com**.

About Our Cover

The development of innovative materials for high-performance optoelectronic devices is critical to the realization of potential advantages that come from organic/polymeric materials, such as cost effective, light weight, flexible, and miniaturization over the traditional silicon and metal components dominated in today's technology node. Herein we show an artist's interpretation of tomorrow's world: artificial organic plants covert solar energy to blooming flowers. Their bright electro-luminescence light attracts a butterfly with wings comprised of organic field effect transistor sheets. Robotic butterfly, luminescent flowers and solar garden have co-evolved as an interlinked e-community, in which their association with each other has resulted in many unique, flexible technological adaptations.

Material Matters™
Vol. 7, No. 1

Aldrich Materials Science
Sigma-Aldrich Co. LLC
6000 N. Teutonia Ave.
Milwaukee, WI 53209, USA

To Place Orders

Telephone	800-325-3010 (USA)
FAX	800-325-5052 (USA)

Customer & Technical Services

Customer Inquiries	800-325-3010
Technical Service	800-231-8327
SAFC®	800-244-1173
Custom Synthesis	800-244-1173
Flavors & Fragrances	800-227-4563
International	414-438-3850
24-Hour Emergency	414-438-3850
Website	sigma-aldrich.com
Email	aldrich@sial.com

Subscriptions

To request your **FREE** subscription to *Material Matters*, please contact us by:

Phone:	800-325-3010 (USA)
Mail:	Attn: Marketing Communications Aldrich Chemical Co., Inc. Sigma-Aldrich Co. LLC P.O. Box 2988 Milwaukee, WI 53201-2988
Website:	Aldrich.com/mm
Email:	sams-usa@sial.com

International customers, please contact your local Sigma-Aldrich office. For worldwide contact information, please see back cover.

Material Matters is also available at Aldrich.com/matsci.

Material Matters (ISSN 1933–9631) is a publication of Aldrich Chemical Co., Inc. Aldrich is a member of the Sigma-Aldrich Group.

Your Materials Matter

Shashi G. Jasty, Ph.D.
Materials Science Initiative Lead

Do you have a compound that you wish Aldrich® Materials Science could list to help materials research? If it is needed to accelerate your research, it matters—send your suggestion to ***matsci@sial.com*** *and we will be happy to give it careful consideration.*

Professor Russell J. Holmes of the University of Minnesota kindly suggested that we offer Spiro-2CBP, (9,9′-(9,9′-spirobi[9*H*-fluorene]-2,7-diyl)bis-9*H*-Carbazole) (**Aldrich Prod. No. 754889**) as a product in our catalog. This molecule is designed as an ambipolar wide energy gap material for use in high performance organic optoelectronic devices. Interestingly, Spiro-2CBP is expected to have a large ionization potential and a small electron affinity. These energy levels could permit this material to be used in organic light-emitting devices (OLEDs) as a host, or potentially an electron/exciton blocking layer to maximize charge confinement and exciton formation. In addition, Spiro-2CBP can also be chemically doped to further improve the film conductivity[1] and can find utility in OLEDs, organic photovoltaic cells (OPVs) and organic laser applications.[2] Carbazole molecules have long been used for as hosts and hole transporting materials due to their high charge carrier mobility, excellent thermal, morphological and photochemical stability. They can be functionalized at *N*-position, linked with other building blocks, such as spirobifluorene.[3]

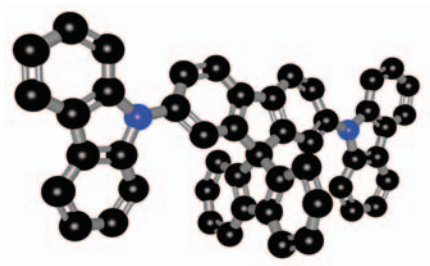

Spiro-2CBP, 97%

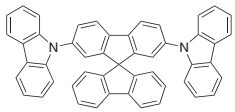

9,9′-(9,9′-Spirobi[9*H*-fluorene]-2,7-diyl)bis-9*H*-carbazole
[924899-38-7] $C_{49}H_{30}N_2$ FW 646.78

754889-250MG	250 mg
754889-1G	1 g

References

(1) Lehnhardt, M.; Hamwi, S.; Hoping, M.; Reinker, J.; Riedl, T.; Kowalsky, W. *Applied Physics Letters* **2010**, *96*, 193301/1.
(2) Nakanotani, Hajime; Akiyama, Seiji; Ohnishi, Dai; Moriwake, Masato; Yahiro, Masayuki; Yoshihara, Toshitada; Tobita, Seiji; Adachi, Chihaya *Advanced Functional Materials* **2007**, *17*, 2328.
(3) Usluer, Ozlem; Demic, Serafettin; Egbe, Daniel A. M.; Birckner, Eckhard; Tozlu, Cem; Pivrikas, Almantas; Ramil, Alberto Montaigne; Sariciftci, Niyazi Serdar *Advanced Functional Materials* **2010**, *20*, 4152.

Table of Contents

Articles

Featured Products

Materials Design Concepts for Efficient Blue OLEDs: A Joint Theoretical and Experimental Study

Evgueni Polikarpov, Asanga B. Padmaperuma
Applied Materials Science Group, Pacific Northwest National Laboratory
Richland, WA 99352 USA

Introduction

Since their discovery,[1] organic light emitting devices (OLEDs) have evolved from a scientific curiosity into a technology with applications in flat panel displays and the potential to revolutionize the lighting market. During their relatively short history, the technology has rapidly advanced, and device efficiencies have increased more than 20-fold, approaching the theoretical limit for internal quantum efficiencies.[2-4] At this point, OLED research moves towards optimization of manufacturing processes, drive circuitry, light extraction, and overall cost reduction. However, discovery of organic materials that provide both operational stability and high efficiency for the devices still remains one of the biggest challenges, particularly for blue emission. In this article, we will describe our approach to design functional OLED materials to meet the complex criteria set forth by device performance goals.

Design of Ambipolar Host Materials for Blue Phosphorescent OLEDs: From Theory to Experiment

The electronic criteria in a given OLED material include charge transport type, charge mobility, boundary orbital energies, and the triplet exciton energy. **Figure 1** shows a schematic of a typical OLED energy diagram that sets the requirements for the position of the boundary orbital energy levels in each type of layer forming the device.

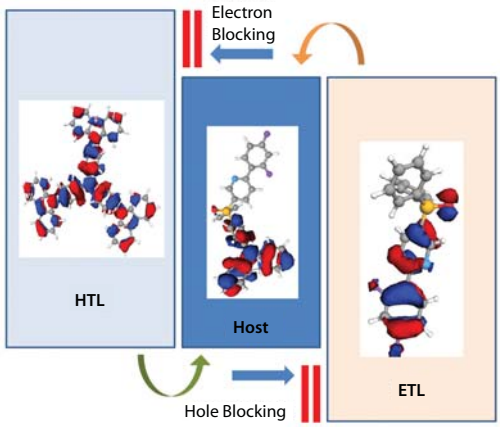

Figure 1. Diagram illustrating the OLED materials design criteria.

The energy diagram demonstrates that hole transport layer materials (HTL) need to have the HOMO level aligned with the corresponding HOMO level of the host to assure the hole flow into the emissive zone with minimal barrier for injection, whereas the HTL LUMO has to be sufficiently high to prevent electron leakage from the host into the HTL. A similar set of rules, but with the opposite sign, exists for the interface of the host with the electron transport layer (ETL): The LUMO levels need to be aligned, and the ETL HOMO sufficiently deep to provide charge confinement. Triplet exciton energies of the materials in both charge transport layers should be significantly higher than the highest triplet level of all the emitters to prevent emissive exciton quenching. The triplet energy constraints also apply to the host materials, but with the requirements less stringent compared to those of hole and electron transport molecules.[5] In addition, the positions of the HOMO of the HTL and LUMO of the ETL will have to match the work functions of both electrodes to minimize charge injection barriers.

The set of energy alignment requirements in a given material can be satisfied by building it from molecular building blocks that carry the desired electronic properties. More often than not, synthesis and device-grade purification of an OLED material are quite resource-intensive. The initial search for an appropriate structure can be initiated based on the known properties of molecular building blocks and chemical intuition. However, methods for screening the proposed materials before synthetic attempts are very valuable. Once we have selected a class of molecules that shows promise for use in OLEDs, the screening and down-selection process involves computational analysis to determine electronic properties of the molecules. Even though the absolute energy values that the computational methods of quantum chemistry can typically provide for relatively large molecules are different from those measured spectroscopically, the information extracted from these calculations is invaluable. For example, trends in electronic properties for large arrays of materials can be used to downselect to a narrower range of suitable candidates to synthesize. In **Figure 2**, we overview a class of host materials obtained as a result of such a downselection approach. The materials are constructed from two types of building blocks, the combination of which provides the host with the ability to transport both electrons and holes. The electron transporting groups are aromatic phosphine oxides and pyridines, whereas either carbazole or arylamine is responsible for hole transport. Succeded by computational evaluation, these materials were then synthesized, characterized, and used in actual devices.[6,7] **Table 1** summarizes the computed and experimental electronic properties of the host materials shown in **Figure 2**.

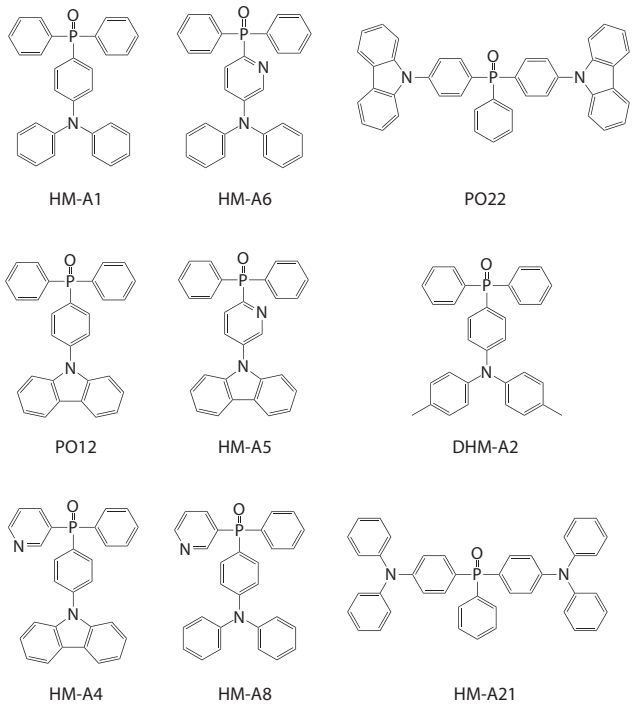

Figure 2. Functionalized phosphine oxide based host materials.

Table 1. Computed and experimentally determined electronic properties of the host materials depicted in **Figure 2**. (All values are in eV.)

	Experimental				Theoretical Predictions [e]				
	From CV		From PL		DFT			TD-DFT	
	E_{HOMO} [a]	E_{LUMO} [b]	E_T [c]	E_S [d]	E_{HOMO}	E_{LUMO}	E_T [f]	E_T [g]	E_S [h]
HM-A1[8]	-5.59	-2.56	2.8	3.4	-5.19	-0.77	3	3.1	3.9
PO12[9]	-5.94	-2.52	2.84	3.6	-5.45	-1.03	3.3	3.2	3.8
HM-A4[6]	-5.85	-2.78	2.99	3.6	-5.55	-1.19	3.2	3.2	3.8
HM-A5[6]	-5.94	-2.91	2.99	3.4	-5.58	-1.19	3.2	3.2	3.8
HM-A6[6]	-5.72	-2.68	2.8	3.29	-1.03	-5.34	3	3.2	3.9
HM-A8[6]	-5.51	-2.69	2.82	3.4	-1.08	-5.27	3	3	3.8
DHM-A2[5]	-5.37	-2.46	2.6	3.3	-0.95	-5.14	3	3	3.8
HM-A21[17]	-5.44	-2.52	2.78	3.4	-5.15	-0.77	3	3	3.8
PO22[17]	-5.9	-2.72	2.99	3.4	-5.5	-1.04	3.3	3.2	3.8

a) Calculated from the oxidation potential using the equation $E_{HOMO} = -1.4*E_{ox} - 4.6$ eV.[10] **b)** Calculated from reduction potentials using a bicarbazole biphenyl (CBP) LUMO as a reference.[11] **c)** Estimated from the photoluminescence of frozen dichloromethane solutions at 77 K. **d)** Estimated from the intersection of the room temperature solution absorption and fluorescence spectra. **e)** Performed using *NWChem* computational package[12] at the B3YLP/6-31G* level. **f)** Estimated from literature.[29] **g)** The lowest energy transition $T_1 \leftarrow S_0$. **h)** The lowest energy non-zero transition $S_1 \leftarrow S_0$.

Comparison of theoretically and experimentally obtained values of molecular energy levels indicates the usefulness of the computations in predicting trends in how individual properties change. The theoretical Density Functional Theory (DFT) method slightly overestimates the orbital energies. However, the absolute values of the experimentally-obtained energies, measured via cyclic voltammetry (CV) in solution, have significant inaccuracy since the test method includes interactions with the solvent and electrodes, not present in operating OLEDs. Therefore, even though stand-alone numbers produced by either of the methods are of limited use, the relative positions of the energy levels in a series of molecules are useful in evaluating the suitability of a given compound as an OLED material compared to its derivatives.

The experiments that were based on theoretical predictions resulted in the synthesis of a series of host materials that allowed for matching of the host properties with other layers in a specific device configuration. These host materials were then evaluated in OLEDs. We have demonstrated previously that the phosphine oxide moiety can be used as the building block for electron transport materials.[13-16] The phosphine oxide-based compound 2,8-bis(diphenylphosphoryl)dibenzothiophene (PO15) is our standard electron transport material due to its favorable electronic structure and relatively high electron mobility. Its LUMO energy level determined by CV is -2.85 eV, which puts PO15 in good energy alignment with most of the host materials shown in **Figure 3**. Its deep HOMO level also provides adequate hole blocking in all cases.

On the other hand, the energy match between 1,1-bis[(di-4-tolylamino) phenyl]cyclohexane (TAPC) (E_{HOMO} = -5.1 eV, E_{LUMO} = -1.7 eV)[5] and some of the hosts such as PO22 is less favorable, which results in decreased charge balance in the emission zone and increased barriers for the hole transport through the interface. This contributes to the EQE decrease in devices with certain hosts such as PO22 (**Figure 3**).

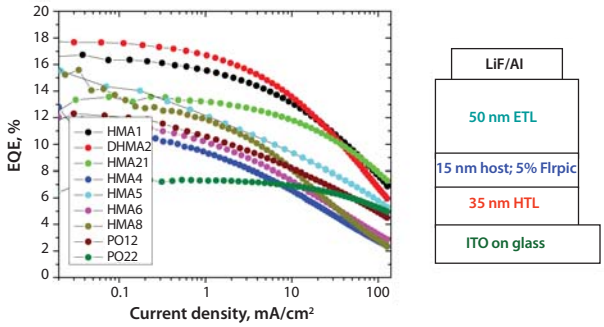

Figure 3. External quantum efficiency vs. current density plots for the devices with host materials from **Table 1** and **Figure 2**, and the corresponding device structure.

Charge Transport in an Organic Material and Reorganization Energy

Even when energy alignment requirements are met, the charge transport within the host remains the main factor that influences charge balance. It has been shown that the charge balance in the emission zone affects the quantum efficiency of the phosphorescent device.[18] To maintain such charge balance, a host material has to support transport of charge carriers of both signs. In addition to the energy level alignment, it is the transport in the host and the charge balance in the emission zone that result in devices with different efficiencies as shown in **Figure 3**.

In addition to thermodynamic effects that define the energy level alignment, the tools of computational quantum chemistry can help predict kinetic parameters that govern charge transport in OLED materials. Here, we attempt to build a library of molecules with high mobility using computed reorganization energies.

Charge transport in organic *p*-conjugated materials at room temperature occurs via a hopping-type mechanism.[19-21] For OLEDs, this mechanism is described as a self-exchange transfer process. The hole-transfer process is described as $M + M^+ \rightarrow M^+ + M$, where M represents a neutral species undergoing charge transfer and M^+ the species containing the hole. Using the standard Marcus model,[22-24] we assume the mobility of a hole or an electron is dominated by the internal reorganization energy, (λ).[25,26] The internal reorganization energy for hole and electron transfer can be expressed as follows:

$$\lambda_{(hole/electron)} = \lambda_1 + \lambda_2 = (E_{(1)}^1 - E_{(0)}^1) + (E_{(0)}^2 - E_{(1)}^2)$$

As shown in **Figure 4**, $E_{(0)}^1$ and $E_{(1)}^2$ are the energies of the neutral and charged (cation/anion) species in their lowest energy geometry, whereas $E_{(1)}^1$ and $E_{(0)}^2$ represent the energies of the neutral and charged (cation/anion), which corresponds to the geometries of the charged (cation/anion) and neutral species, respectively.

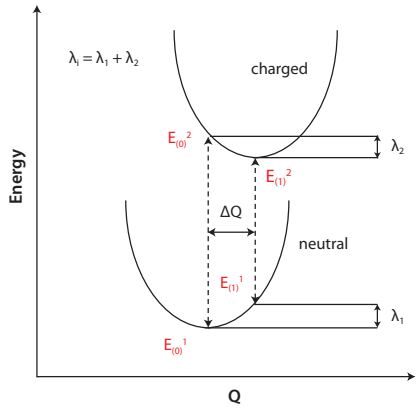

Figure 4. Energy vs. Reaction (Q) coordinate scheme to illustrate reorganization energy calculations. See text for notations.

Smaller reorganization energies allow for lower energy barriers in the elementary step of electron transfer reactions. Such a reduced energy barrier results in higher charge mobility and is consistent with published reports.[27] The correlation between our computed reorganization energies and experimentally determined hole mobilities available in published literature[28] for a series of commonly used hole transporting materials for OLEDs is shown below in **Figure 5**. Though the trend is not perfectly linear, it is evident that as the reorganization energy decreases, the charge mobility increases. As expected there is good agreement between computed and experimentally determined values.

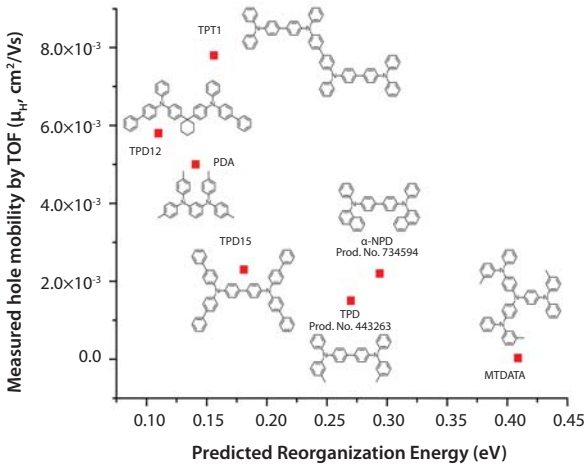

Figure 5. Time of flight mobilities[27] vs. reorganization energies computed in this work for common OLED hole transport materials.

Case Study: Host and Electron Transport Organic Materials with Deep LUMO Levels

Next, we will illustrate the use of the tools developed to design a family of host and electron transport/hole blocking materials with predetermined electronic properties. Sometimes it is desirable to have a deep LUMO in a host material to match a specific ETL and/or reduce the possibility of electron leakage into the HTL. On the other hand, the reasons for an ETL material to have a deep LUMO level can include energy level alignment with a specific cathode work function or ability to utilize *n*-doping by compounds with reasonable chemical stability. The approach to building host and ETL materials with deep LUMO levels can be based on the general principles described above for the design of ambipolar hosts. In this case study, the functional groups comprising the target molecule should provide a) the needed charge transport properties (ambipolar for the hosts, and electron-transporting for the ETLs), and b) electronic effects that allow for energy level shift. **Figure 6** lists the prospective candidates that may satisfy the charge transport and LUMO alignment conditions.

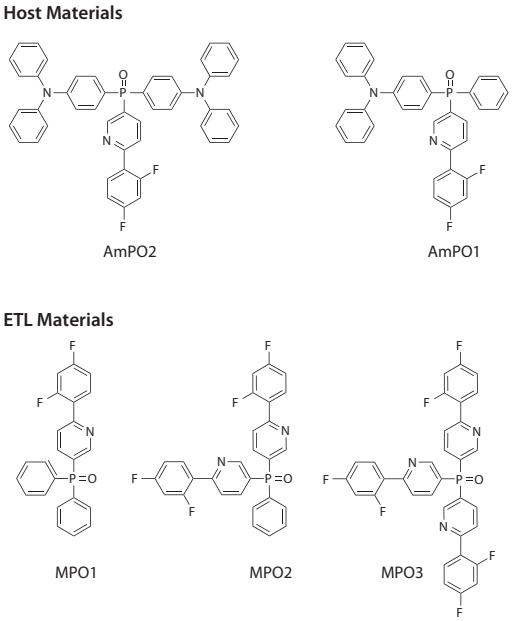

Figure 6. Difluorophenylpyridine-substituted phosphine oxide (DFppy-PO) host (top) and ETL (bottom) materials.

The chemical structures in **Figure 6** were subject to geometry optimization, time-dependent DFT analysis to estimate the triplet level positions,[29] and reorganization energy calculations,[30] which allowed for prediction of the device-relevant molecular properties. We chose to build the molecules from the electron-transporting phosphine oxide moieties, hole-transporting arylamines, and difluorophenylpyridine (DFppy) groups that will provide the desired LUMO shift. The boundary molecular orbitals included in **Figure 7** demonstrate the effect of this building strategy.

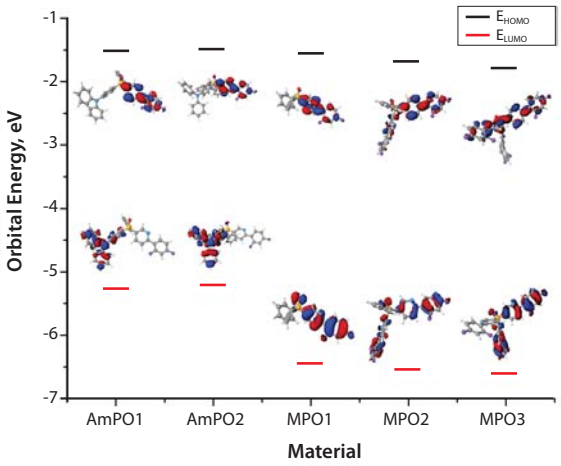

Figure 7. Computed electron density maps and orbital energies for the DFppy-PO host and ETL materials

The two materials on the left (AmPO1 and AmPO2) are the hosts that should provide ambipolar charge transport. Their HOMO is localized on the arylamine fragment, whereas the LUMO is entirely defined by the dFppy unit. Therefore, the goal of providing a deep LUMO level for these materials is achieved by the choice of a functional group with a deep LUMO on which the LUMO of the entire molecule will be localized. The same holds true for the LUMO levels of the three ETL materials shown on the right in **Figure 7**. Unlike the hosts, there are no functional groups with shallow HOMO levels on the ETL molecules. In fact, both boundary orbitals of the ETLs are localized on the difluorophenylpyridine fragment. The HOMO energy of difluorophenylpyridine is quite low. It translates into good hole-blocking properties expected from the dFppy-based ETLs discussed here. The theoretically predicted electronic properties for the dFppy-substituted hosts and ETLs are listed in **Table 2** below.

Table 2. Computed energy levels and reorganization energies for dfppy-PO host and ETL materials. (All values reported in eV.)

	E_{HOMO}	E_{LUMO}	Hole			Electron			E_T
			λ1	λ2	$\lambda_{(hole)}$	λ_1	λ_2	$\lambda_{electron}$	
AmPO1	-1.52	-5.27	0.1045	0.0976	0.2021	0.293	0.251	0.544	2.99
AmPO2	-1.49	-5.21	0.0554	0.0536	0.109	0.246	0.171	0.417	3.01
MPO1	-1.55	-6.46	0.2052	0.3031	0.5083	0.259	0.25	0.509	2.92
MPO2	-1.68	-6.55	0.1345	0.1281	0.2626	0.217	0.147	0.364	2.92
MPO3	-1.79	-6.61	0.143	0.0973	0.2404	0.168	0.104	0.272	2.92

Conclusions

We reported on the methodology to design functional organic materials for OLEDs. Host and charge transport materials can be synthesized by combination of molecular building blocks that provide the necessary electronic properties. We showed how the correlation between theoretical predictions and the measured electrochemical and photophysical data allow for streamlining the OLED material design and down-selection process with examples from our recent research.

References

(1) Tang, C.W.; VanSlyke, S.A. *Appl. Phys. Lett.* **1987**, *51*, 913.
(2) Wang, Z. B.; Helander, M. G.; Qiu, J.; Puzzo, D. P.; Greiner, M. T.; Hudson, Z. M.; Wang, S.;Liu, Z. W.; Lu Z. H. Nature Photonics **2011**, doi: 10.1038/nphoton.2011.259
(3) Reineke, S.; Lindner, F.; Schwartz, G.; Seidler, N.; Walzer, K.; Luessem, B.; Leo, K. *Nature* **2009**, *459*, 234.
(4) Adachi, C.; Baldo, M. A.; Thompson, M. E.; Forrest, S. R. *J. Appl. Phys.* **2001**, *90*, 5048.
(5) Swensen, J. S.; Polikarpov, E.; Von Ruden, A. L.; Wang, L.; Sapochak, L. S.; Padmaperuma, A. B. *Adv. Funct. Mat.* **2011**, *21*, 3250.
(6) Koech, P. K.; Polikarpov, E. V.; Rainbolt, J. E.; Cosimbescu, L.; Swensen, J. S.; Von Ruden, A. L.; Padmaperuma, A. B. *Org. Lett.* **2010**, *12*, 5534.
(7) Polikarpov, E.; Swensen, J. S.; Cosimbescu,L.; Koech, P.; Rainbolt, J. E.; Padmaperuma, A. B. *Appl. Phys. Lett.* **2010**, *96*, 053306.
(8) Polikarpov, E.; Swensen, J. S.; Chopra, N.; So, F.; Padmaperuma, A. B. *Appl. Phys. Lett.* **2009**, *94*, 223304.
(9) Sapochak, L. S.; Padmaperuma, A.B.; Cai, X.; Male, J.L.; Burrows, P.E. *J. Phys. Chem. C*, **2008**, *112*, 7989.
(10) D'Andrade, B. W.; Datta, S.; Forrest, S. R.; Djurovich, P. I.; Polikarpov, E.; Thompson, M. E. *Org. Electr.* **2005**, *6*, 11.
(11) Kolosov, D.; Adamovich, V.; Djurovich, P. I.; Thompson, M. E.; Adachi, C. *J. Am. Chem. Soc.* **2002**, *124*, 9945.
(12) Bylaska, E. J. et al. "NWChem, A Computational Chemistry Package for Parallel Computer, Version 5.1" (**2007**), Pacific Northwest National Laboratory, Richland, Washington 99352-0999, USA. A modified version.
(13) Padmaperuma, A. S.; Sapochak, L. S.; Burrows, P. E. *Chem. Mater.* **2006**, *18*, 2389.
(14) Cai, X.; Padmaperuma, A. B.; Sapochak, L. S.; Vecchi, P. A.; Burrows, P. E. *Appl. Phys. Lett.* **2008**, *92*, 083308.
(15) Burrows, P. E.; Padmaperuma, A. B.; Sapochak, L. S.; Djurovich, P. I.; Thompson, M. E. *Appl. Phys. Lett.* **2006**, *88*, 183503.
(16) Vecchi, P. A.; Padmaperuma, A. B.; Qiao, H.; Sapochak, L. S.; Burrows, P. E. *Org. Lett.* **2006**, *8*, 4211.
(17) Cosimbescu, L.; Polikarpov, E.; Swensen, J. S.; Darsell, J. T.; Padmaperuma, A. B. *Journal of SID* **2011**, *19*, 353.
(18) Giebink, N. C.; Forrest, S. R.; *Phys. Rev. B* 2008, **77** (23), 235215.
(19) Hutchison, G. R.; Ratner, M. A.; Marks, T. J. *J. Am. Chem. Soc.* **2005**, *127*, 2339.
(20) Epstein, A. J.; Lee, W. P.; Prigodin, V. N. *Synth. Met.* **2001**, *117*, 9.
(21) Reedijk, J. A.; Martens, H. C. F.; van Bohemen, S. M. C.; Hilt, O.; Brom, H. B.; Michels, M. A. J. *Synth. Met.* **1999**, *101*, 475.
(22) Marcus, R. A. *J. Chem. Phys.* **1965**, *43*, 679.
(23) Marcus, R. A. *Rev. Mod. Phys.* **1993**, *65*, 599.
(24) Hutchinson, G. R.; Ratner, M. A.; Marks, T. J. *J. Am. Chem. Soc.* **2005**, *127*, 2339.
(25) Nelsen, S. F.; Trieber, D. A.; Ismagilov, R. F.; Teki, Y. *J. Am. Chem. Soc.* **2001**, *123*, 5684.
(26) Nelsen, S. F.; Blomgren, F. *J. Org. Chem.* **2001**, *66*, 6551
(27) Sokolov, A. N.; Atahan-Evrenk, S.; Mondal, R.; Akkerman, H. B.; Sánchez-Carrera, R. S.; Granados-Focil, S.; Schrier, J.; Mannsfeld, S. C. B.; Zoombelt, A. P.; Bao, Z.; Aspuru-Guzik, A. *Nat. Commun.* **2011**, 2:437 doi: 10.1038/ncomms1451.
(28) Aonuma, M.; Oyamada, T.; Sasabe, H.; Miki, T.; Adachi, C. *Appl. Phys. Lett.* **2007**, *90*, 183503.
(29) Kim, D.; Salman, S.; Coropceanu, V.; Salomon, E; Sapochak, L. S.; Kahn, A.; Bredas, J. L. *Chem. Mater.* **2010**, *22*, 247.
(30) Sakanoue, K.; Motoda, M.; Sugimoto, M.; Sakaki, S. *J. Phys. Chem. A* **1999**, *103*, 5551.

Emitters for Host Materials

Name	Structure	Purity	UV Data	Prod. No.
Tris[2-phenylpyridinato-C^2,*N*]iridium(III), sublimed grade (Ir(ppy)$_3$)		~97%	λ_{abs} 282 nm λ_{max} 305/507 nm in chloroform	694924-250MG
Tris[2-(4,6-difluorophenyl)pyridinato-C^2,*N*] iridium(III) (Ir(Fppy)$_3$)		96%	λ_{abs} 347 nm λ_{max} 290/480 nm in chloroform	682594-250MG
Tris[1-phenylisoquinoline-C^2,*N*]iridium(III), sublimed grade (Ir(piq)$_3$)		~99%	λ_{abs} 324 nm λ_{max} 324/615 nm in THF	688118-250MG
Tris[2-(benzo[*b*]thiophen-2-yl)pyridinato-C^3,*N*] iridium(III) (*fac*-Ir(btpy)$_3$)	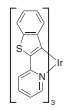	96%	λ_{abs} 324 nm λ_{max} 330/595 nm in chloroform	680877-250MG
Dichlorotetrakis(2-(2-pyridinyl)phenyl) diiridium(III) ([(ppy)2IrCl]2)	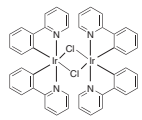	≥95% (HPLC)	-	658383-100MG 658383-500MG
Bis(8-hydroxy-2-methylquinoline)-(4-phenyl phenoxy)aluminum (BAlq)	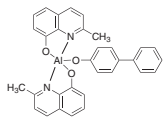	95%	λ_{abs} 259 nm λ_{max} 334, 477 nm in THF	704571-5G
Tris-(8-hydroxyquinoline)aluminum, sublimed grade (Alq$_3$)	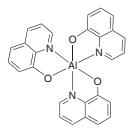	99.995% trace metals basis	λ_{abs} 259 nm λ_{max} 390/519 nm	697737-1G 697737-5G

Name	Structure	Purity	UV Data	Prod. No.
Tris(2,2′-bipyridyl-d_8)ruthenium(II) hexafluorophosphate	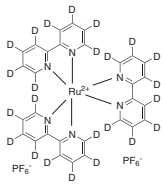	95%	-	652407-100MG
Platinum octaethylporphyrin (PtOEP)	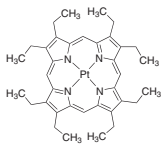	98% Dye Content	λ_{abs} 381 nm	673625-100MG
Copper(II) phthalocyanine, triple-sublimed grade (CuPc)	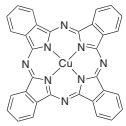	>99.99% trace metals basis	λ_{abs} 678 nm λ_{max} 404 nm	702854-500MG

Hole Transport Materials

For a complete list of available products, including Electron Transport Materials, visit Aldrich.com/oel

Name	Structure	Purity	Prod. No.
DH-FTTF (5,5′-Bis(7-hexyl-9*H*-fluoren-2-yl)-2,2′-bithiophene	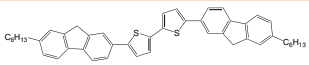	-	754064-250MG
DBP (Dibenzo{[f,f′]-4,4′,7,7′-tetraphenyl}diindeno[1,2,3-cd:1′,2′,3′-lm] perylene)	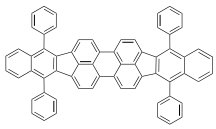	>99%, HPLC	753939-250MG
N,N′-Di-[(1-naphthyl)-*N,N*′-diphenyl]-1,1′-biphenyl)-4,4′-diamine (NPD; NPB)	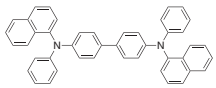	96%	734594-5G
1,3-Bis(*N*-carbazolyl)benzene (1,3-Di(9*H*-carbazol-9-yl)benzene; mCP)	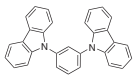	97%	701874-5G
4,4′-Bis(*N*-carbazolyl)-1,1′-biphenyl (4,4′-Bis(9-carbazolyl)-1,1′-biphenyl; CBP) sublimed grade	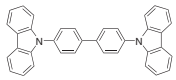	99.9% trace metals basis	699195-1G 699195-5G
Bathocuproine (BCP)	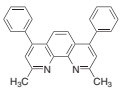	99.99% trace metals basis	699152-500MG 699152-5G
3-(Biphenyl-4-yl)-5-(4-*tert*-butylphenyl)-4-phenyl-4*H*-1,2,4-triazole (TAZ)	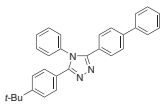	97%	685720-1G
3,5-Bis(4-*tert*-butylphenyl)-4-phenyl-4*H*-1,2,4-triazole	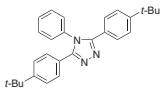	97%	685682-1G
N,N′-Diphenyl-*N,N*′-di-*p*-tolylbenzene-1,4-diamine	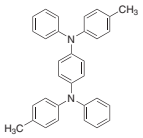	~97%	663263-1G 663263-5G

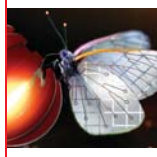

Name	Structure	Purity	Prod. No.
1,3,5-Tris(2-(9-ethylcabazyl-3)ethylene)benzene (TECEB)	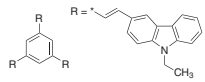	~97%	661732-500MG
4,4′-Bis(*N*-carbazolyl)-1,1′-biphenyl (DCBP)	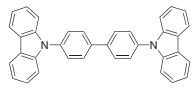	97%	660124-1G 660124-5G
Bathophenanthroline (BPhen)	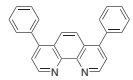	97%	133159-500MG 133159-1G
Poly(thiophene-3-[2-(2-methoxyethoxy)ethoxy]-2,5-diyl), sulfonated solution (Plexcore® OC RG-1100)	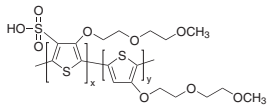	-	699799-25ML
Poly(thiophene-3-[2-(2-methoxyethoxy)ethoxy]-2,5-diyl), sulfonated solution (Plexcore® OC RG-1200)	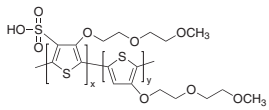	-	699780-25ML
Poly[(9,9-di-*n*-octylfluorenyl-2,7-diyl)-*alt*-(benzo[2,1,3]thiadiazol-4,8-diyl)] (F8BT) average M_n 10,000-20,000	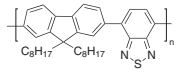	-	698687-250MG
Poly(3-decyloxythiophene-2,5-diyl)	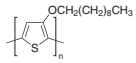	-	693391-500MG
Poly[(9,9-dihexylfluoren-2,7-diyl)-*co*-(anthracen-9,10-diyl)]	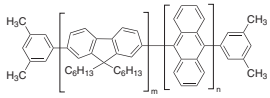	-	685712-500MG
Poly[(9,9-dihexylfluoren-2,7-diyl)-*co*-(9-ethylcarbazol-2,7-diyl)] (PFH-EC)	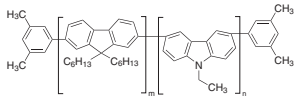	-	685704-500MG
Poly[tris(2,5-bis(hexyloxy)-1,4-phenylenevinylene)-*alt*-(1,3-phenylenevinylene)] (PTDPV)	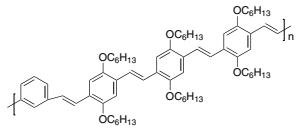	-	664936-500MG
Poly(2-vinylcarbazole)	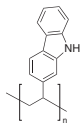	-	649287-500MG
Poly(2,5-di(3,7-dimethyloctyloxy)cyanoterephthalylidene)	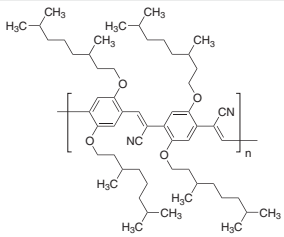	-	646571-250MG
Poly(2,5-didodecylphenylene-1,4-ethynylene)	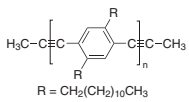	-	637009-500MG

ALDRICH Materials Science

Highly Absorbing Squaraines and Their Application to Organic Photovoltaics

Siyi Wang,† Mark E. Thompson,† and Kanth V.B. Josyula‡
†Department of Chemistry, University of Southern California, Los Angeles, CA 90089
‡New Products R&D, Sigma-Aldrich Co. LLC, 6000 N. Teutonia Ave, Milwaukee, WI 53209

Organic Photovoltaics (OPVs) have attracted a great deal of research interest as they are potentially low cost, lightweight, and flexible sources for renewable energy. Exploring new materials is one of the critical approaches to achieve high-performance OPVs in solar cell research. This article describes squaraine dyes as highly efficient absorbers for OPV applications.

Squaraines are 1,3 derivatives of squaric acid, a condensation product of squaric acid and electron-rich aromatics or heterocycles. Squaraine dyes feature sharp and intense solution absorption in the red to near infrared (NIR) region of the solar spectrum. More importantly, squaraine film absorption is quite broad, which is highly beneficial for sunlight absorption. A series of novel, high purity squaraines have recently been prepared, including the products in the table below.[1] 2,4-bis[4-(*N*,*N*-diisobutylamino)-2,6-dihydroxyphenyl] squaraine (SQ, **Aldrich Prod. No. 758337**) has been successfully utilized as a donor material for high-performance cells in both vacuum-deposited and solution-processed OPVs.[2] Pairing SQ with PC_{70}, C_{70}-fullerene acceptor, has achieved high power conversion efficiency of 5.5% mainly due to its high open circuit voltage, high short circuit current, and high fill factor.[3] Replacing diisobutylamino substituents with diphenyl amino moieties, 2,4-bis[4-(*N*,*N*-diphenylamino)-2,6-dihydroxyphenyl] squaraine (DPSQ, **Aldrich Prod. No. 757233**), improved solubility for solution-processing of OPVs with enhanced charge carrier mobility. DPSQ, with its 0.2 eV deeper HOMO energy than SQ, is anticipated to lead to OPV devices with higher open circuit voltage and hence better device performance (Figure 1).[4]

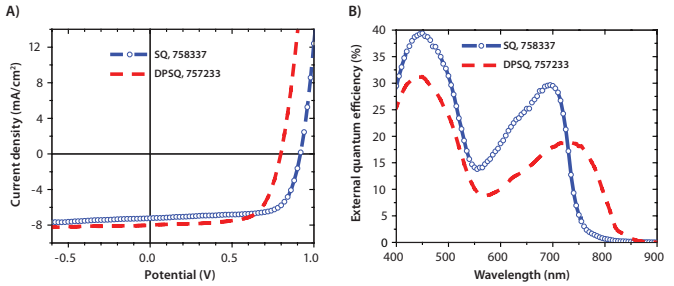

Figure 1. A) current density (*J*) versus voltage (*V*) characteristics at 1 sun illumination of the as-cast SQ/C_{60} and DPSQ/C_{60} cells with structure of ITO/MoO3(80 Å)/SQs(85 ± 5 Å)/C_{60}(400 Å)/3,4,9,10 perylenetetracarboxylic bisbenzimidazole (PTCBI) (80 Å)/Ag (1,000 Å) and **B)** External quantum efficiencies (*EQE*) plot.

In summary, initial studies of these squaraine derivatives utilized as absorbers in OPV devices showed enhanced charge carrier mobility and higher open circuit voltage, compared to previously studied squaraines. Further optimization of device performance using this class of small molecules is in progress.

References

(1) Wang, S. Y.; Hall, L.; Diev, V. V.; Haiges, R.; Wei, G. D.; Xiao, X.; Djurovich,P. I.; Forrest, S. R.; Thompson, M. E., *Chem. Mater.*, **2011**, *23*, 4789.
(2) Wang, S. Y.; Mayo, E. I.; Perez, M. D.; Griffe, L.; Wei, G. D.; Djurovich, P. I.; Forrest, S. R.; Thompson, M. E., *Appl. Phys. Lett.*, **2009**, *94*, 233304.
(3) Wei, G. D.; Wang, S. Y.; Sun, K.; Thompson, M. E.; Forrest, S. R., *Adv. Energy Mater.*, **2011**, *1*, 184.
(4) Wei, G. D.; Xiao, X.; Wang, S. Y.; Sun, K.; Bergemann, K. J.; Thompson, M. E.; Forrest, S. R., Manuscript in preparation., **2011**.

Description	Structure	Prod. No.
2,4-bis[4-(*N*,*N*-diisobutylamino)-2,6-dihydroxyphenyl] squaraine (SQ)	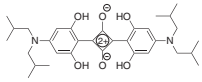	**758337-1G**
2,4-bis[4-(*N*,*N*-diphenylamino)-2,6-dihydroxyphenyl] squaraine (DPSQ)	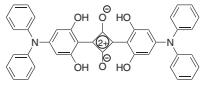	**757233-1G**
2,4-bis[4-(*N*,*N*-dibenzylamino)-2,6-dihydroxyphenyl] squaraine (DBSQ)	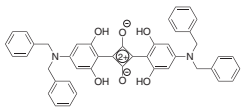	**757268-1G**

To browse our Organic Electronics materials, visit **Aldrich.com/oel**

Optoelectronic Devices Based on Diketopyrrolopyrrole (DPP)-containing Conjugated Small Molecules

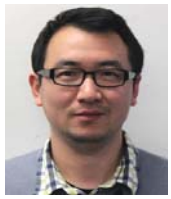

Jianhua Liu and Thuc-Quyen Nguyen*
Center for Polymers and Organic Solids
Department of Chemistry & Biochemistry
University of California, Santa Barbara, California 93106, United States
*Email: quyen@chem.ucsb.edu

Introduction

Optoelectronic devices such as light-emitting diodes (LEDs), solar cells, and light-emitting field effect transistors (FETs) that utilize organic materials as their light harvesting and/or charge transporting component have recently been the subject of much academic and commercial attention.[1,2] This widespread interest is motivated by organic materials' unique advantages compared to their inorganic counterparts, e.g., low-cost, lightweight, solution processable, and compatible with flexible substrates. Conjugated polymers are the most-widely investigated class of organic materials for these applications.[3,4] Organic solar cells based on a conjugated polymers[5] or small molecule/fullerene derivative blends have achieved a power conversion efficiency (PCE) up to 10%. In addition, FETs utilizing conjugated polymers as the charge transporting layer have demonstrated carrier mobilities up to 2.0–3.0 $cm^2V^{-1}s^{-1}$ making them competitive with lower performing inorganic materials such as amorphous silicon.[6,7] Conjugated small molecules have also historically been successfully used in FETs with pentacene and its soluble derivatives among the most studied such materials.[8] Recently, a solar cell comprised of a soluble conjugated small molecule/fullerene blend achieved a PCE of 6.7%,[9] narrowing the performance gap between organic solar cells made from conjugated polymers and conjugated small molecules. Compared to conjugated polymers, small molecules have several advantages such as well-defined structures, ease of synthesis and functionalization, no batch-to-batch variations, and the ability to use standard purification techniques.[10] In addition, crystal structures of small molecules can be readily obtained by X-ray crystallography, providing an efficient approach to probe structure-property relationships, which is essential for designing new materials.[11,12]

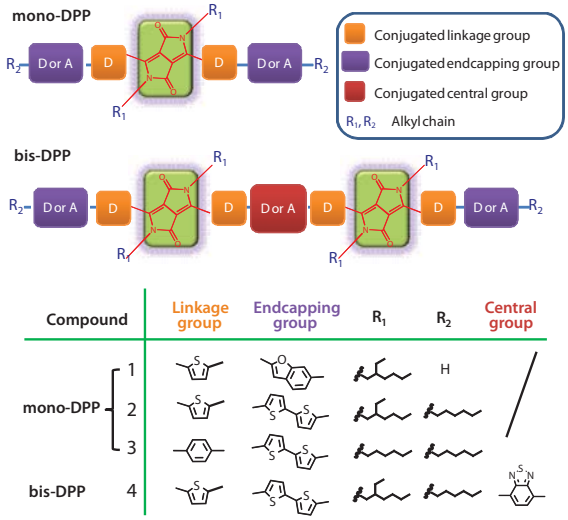

Figure 1. General molecular architectures of mono-DPP and bis-DPP small molecular compounds (upper) and four specific examples (mono-DPP: compounds 1-3; bis-DPP: compound 4 with different building blocks (bottom). D and A represent the electronic donating (D) and electronic accepting (A) properties that the building blocks may have.

A useful strategy for synthesizing conjugated small molecules for use in optoelectronic devices is to begin with a chromophore that can absorb most of the visible region of the solar spectrum. Diketopyrrolopyrrole (DPP) is such a chromophore and is also a desirable molecular building block because of its chemical stability, and ease of synthesis and modification. **Figure 1** shows the general molecular architectures of DPP-containing small molecules synthesized in our lab. These compounds are classified into two subgroups: mono-DPPs which have only one DPP unit and bis-DPPs which have two DPP units. Due to the electron deficiency of the lactam structure in DPP, electron donating functional groups such as thienyl and phenyl derivatives are selected to incorporate with DPP as linkage and endcapping groups to further tune properties such as the optical band gap, highest occupied molecular orbital (HOMO), and lowest unoccupied molecular orbital (LUMO) levels. Alkyl chains are introduced on the conjugated backbone to induce solubility in common organic solvents, and to modify the degree of crystallinity and specific packing motif. Additionally, central groups in bis-DPP compounds provide a further structural handle capable of modifying material properties. This combination of different side chains and central, linkage, and endcapping groups allows the resultant material's optoelectronic properties to be tuned with a high degree of sensitivity. This tunability enables engineering of the material properties necessary for optimal performance in optoelectronic devices. A number of DPP-containing derivatives have been synthesized by our group and several other groups.[13-19] In **Figure 1**, we highlight several specific examples of DPP-containing conjugated small molecules for use in organic solar cells (compounds 1–3) and FETs (compound 4).

Synthesis

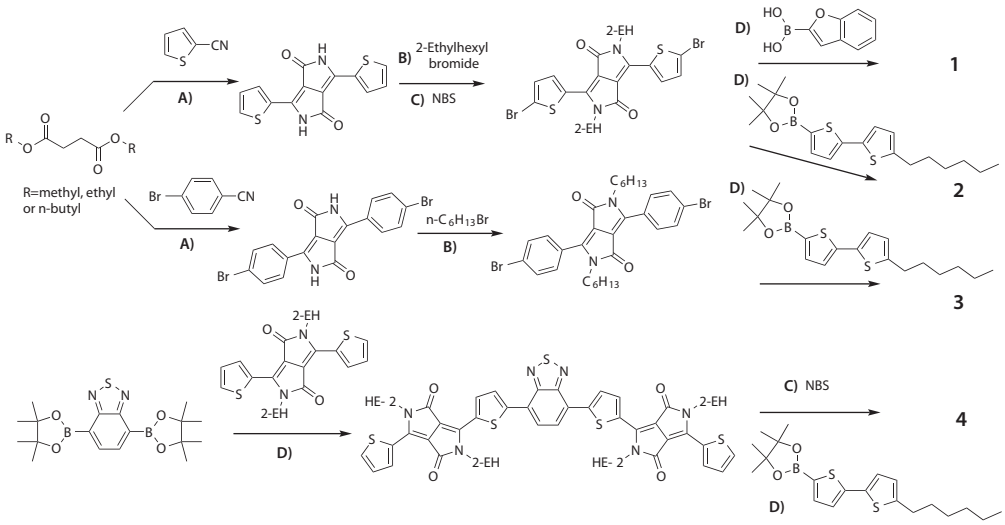

Scheme 1. Divergent synthetic routes of DPP-containing conjugated small molecules. **A)** Potassium t-butoxide, 2-methyl-2-butanol, reflux 5 h; **B)** K_2CO_3, DMF reflux 12 h; **C)** $CHCl_3$, RT, 12 h; **D)** $Pd_2(dba)_3$, K_3PO_4, THF/H_2O, 70 °C 12 h.

The DPP-containing small molecules displayed in **Figure 1** are synthesized by the divergent approach illustrated in **Scheme 1**. For the mono-DPPs (compounds 1–3), this approach consists of several reaction steps such as DPP-linkage formation, N-alkylation, linkage bromination, and endcap group coupling. When the linkage group is a thienyl group, the DPP-thiophene can be prepared by a single reaction of a thienyl nitrile with a succinic diester. The resultant DPP-thiophene precursor is not soluble in organic solvents due to its internal hydrogen bonds. N-alkylation of the DPP-thiophene precursor with an alkyl bromide makes the precursor soluble enough for the subsequent modifications. The following bromination with N-bromosuccinimide (NBS) provides the thienyl groups with the reactive sites necessary to complete the final endcap group coupling. This final step can be achieved via a palladium-catalyzed Suzuki or Stille coupling. When the linkage is a phenyl group, the above bromination step can be omitted by using bromobenzonitrile as the starting material. For the bis-DPPs, the divergent approach usually consists of iterative Suzuki or Stille couplings. Taking compound 4 as an example, an intermediate is synthesized by reacting an active benzothiadiazole (BT) precusor (benzothiadiazole-bis(boronic acid piancol ester)) with a mono-brominated DPP-thiophene via Suzuki coupling. The obtained intermediate is then brominated by NBS and subsequently reacted with an endcapping group via Suzuki coupling, generating compound 4. It is important to note the purity of the final material is critical for optimal device performance. It has been our experience that the presence of even a small amount of impurity can negatively affect the performance of a device. Therefore, both molecular design and precise purification are essential for synthesis of conjugated small molecules for high-performing optoelectronic devices.

Organic Bulk Heterojunction Solar Cells

In order for a material to be successfully used in a solar cell, its optical absorption profile must have a large overlap with the terrestrial solar spectrum. **Figure 2A** shows the pristine film absorption spectra of compounds 1–3. Their absorption edges extend to 670 nm, 704 nm and 775 nm, respectively. Due to its longer backbone conjugation length, compound 2 has a larger absorption edge than compound 1. Replacing the thienyl linkage with a phenyl linkage (compound 3) leads to a blue shift of approximately 105 nm. A twist conformation between the neighboring DPP and phenyl moieties has been confirmed from the single crystal structure of compound 3. This twist conformation reduces the effective conjugation length of the molecule and is likely the cause of this large blue shift in optical absorption.

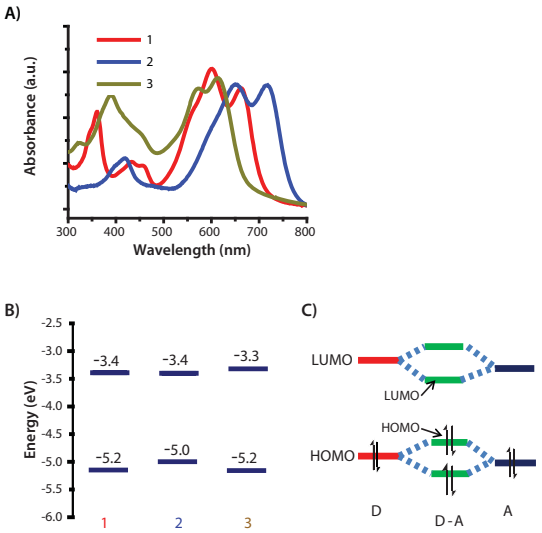

Figure 2. A) Normalized UV-Vis pristine film absorption and **B)** HOMO/LUMO energy levels of compounds 1-3. **C)** A simplified molecular orbital hybridization from donor-acceptor moieties in a D-A molecule.

In addition to optical absorption, the HOMO and LUMO levels also play an important role in determining solar cell performance. **Figure 2B** shows the HOMO and LUMO energy diagrams of three compounds. The HOMO levels are determined by ultraviolet photoelectron spectroscopy (UPS) and the LUMO levels are calculated using the relationship LUMO = HOMO + E_g, where E_g is the optical energy bandgap estimated from UV-Vis film absorption cutoff. Compound 2 has the highest HOMO level (-5.0 eV) while the other two have the same value (-5.2 eV). Unlike the HOMO levels, the LUMO level of compound 3 is highest (-3.3 eV) while the others have a similar level (-3.4 eV). The differences among HOMO and LUMO levels can be explained using a simple model of molecular orbital hybridization as illustrated in **Figure 2C**. The DPP-containing compounds discussed here have a donor (D)–acceptor (A) or push-pull structure, where the DPP is the acceptor motif and thiophenes are the donor motif. The molecular orbital hybridization between the donor and acceptor motifs reduces the energy band gap of a D–A molecule. Furthermore, the HOMO and LUMO levels of a D–A molecule are dominated by the HOMO of the donor motif and the LUMO of the acceptor motif, respectively. Therefore, compound 2 has a higher HOMO value because it has a stronger donor motif (more thiophene rings). Compound 1 and 2 have the same LUMO value due to their use of the same acceptor motif. The twisted conformation between DPP and phenyl groups in compound 3 reduces D–A orbital hybridization and results in a deeper HOMO and a higher LUMO as compared with compound 2.

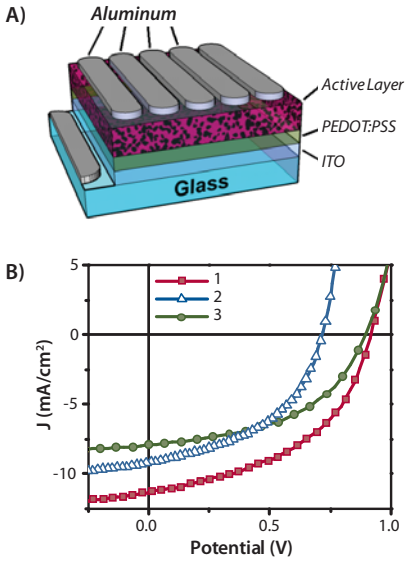

Figure 3. A) A schematic illustration of an organic solar cell device. **B)** Typical *J-V* curves of optimized solar cell devices fabricated using compounds 1-3 as donors with $PC_{71}BM$ as the acceptor (donor/acceptor mass ratio: 60:40).[13-15,20]

Solar cells using compounds 1–3 as donor materials were fabricated with a standard architecture of indium tin oxide (ITO)/ Poly(3,4-ethylenedioxythiophene) poly(styrenesulfonate) (PEDOT:PSS)/a DPP-containing compound:[6,6]-phenyl C_{71}-butyric acid methyl ester ($PC_{71}BM$)/Al as shown in **Figure 3A**. Typical current density-voltage (*J-V*) curves of optimized devices under one sun irradiation (AM 1.5/100 $mWcm^{-2}$) are presented in **Figure 3B**. The corresponding device performance parameters are listed in **Table 1**. Solar cell devices made from compound 1/$PC_{71}BM$ blends have the best performance (with a peak power conversion efficiency [PCE] of 4.8%) due to having high open circuit voltage (V_{oc}) and short circuit current density (J_{sc}).[15,20] Under low light intensity, a PCE of up to 5.2% can be achieved.[21] Although the PCE value of the DPP material reported by our group in 2009 was lower as compared to some conjugated polymer solar cells, it has stirred a lot of interest in the community to pursue solution-processed small molecules as alternative donor materials in bulk heterojunction solar cells. Within two years, a new material having a PCE of 6.7% have been reported by Bazan and Heeger (UCSB)[9] and the PCE of 10% reported by the Mitsubishi Chemical at the Fall 2011 Materials Research Society meeting in Boston is based on solution-processed small molecules.

Table 1. Summary of solar cell characteristics of optimized devices

Compound	V_{oc} (V)	J_{sc} (mA/cm^2)	FF	PCE (%)
1	0.92	11.3	0.46	4.8
2	0.75	9.2	0.44	3
3	0.9	7.9	0.49	3.4

In a bulk heterojunction solar cell, the V_{oc} is usually determined by the HOMO level of the donor material ($HOMO_{donor}$) and the LUMO level of the acceptor material ($LUMO_{acceptor}$), which can be described with the empirical equation $V_{oc} \cong (1/e)$ ($|HOMO_{donor}|$-$|LUMO_{acceptor}|$) - 0.3.[22] Therefore, compounds 1 and 3 have a similar V_{oc} because of their similar HOMO levels. The higher HOMO level of compound 2 results in a lower V_{oc}. For the J_{sc}, the donor material that has a lower bandgap (larger absorption edge) theoretically would have a higher J_{sc} if similar charge recombination and trapping rates are assumed. This might be the reason for the higher J_{sc} of compound 1 compared to compound 3. Compound 2 has a lower J_{sc} than expected. We hypothesize this low J_{sc} might be the result of an undesirable film morphology and quality. **Figure 4** shows the AFM height images of active layers in these optimized solar cell devices. The blend films of compounds 1/$PC_{71}BM$ and compound 3/$PC_{71}BM$ have similar morphologies which consist of rod-like crystalline domains with a good size distribution, while the compound 2/$PC_{71}BM$ blend film has a poor morphology with uneven domains and unclear boundaries. The root mean square roughness (R_{RMS}) of these films highlighted in **Figure 4** indicates a poor film quality of compound 2/$PC_{71}BM$ blends (the highest R_{RMS}). The poor film morphology and quality of compound 2/$PC_{71}BM$ blends could increase the rate of various recombination and trapping processes during solar cell operation, leading to a low J_{sc}.

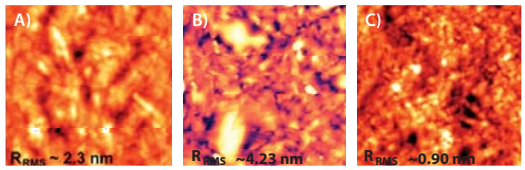

Figure 4. Tapping-mode AFM height images of Compound 1/$PC_{71}BM$ **(A)**, Compound 2/$PC_{71}BM$ **(B)**, and Compound 3/$PC_{71}BM$ **(C)** blend films from optimized solar cells. Scan size: 2 µm × 2 µm.

Fill factors (*FF*s) of optimized devices range from 0.44–0.49, which are typical values for solar cells made from solution-processed conjugated small molecules and smaller than typical values of polymeric solar cells (>0.6). Overall, solar cells made from current mono-DPPs have lower *FF*s and J_{sc}s compared to other optimal devices made from conjugated polymers;[5] although, it is possible to improve the *FF* of solution-processed small molecule solar cells using metal oxide to replace PEDOT:PSS layer.[9] A potentially useful strategy to improve the PCE of DPP-containing conjugated small molecule solar cells is to increase the size of the conjugated molecules, which can be achieved by making bis-DPP compounds as displayed in **Figure 1**. Conjugated building blocks widely used in conjugated polymers, such as dithieno[3,2-b;2′3′-d]silole (SDT), benzo[1,2-b:4,5-b′]dithiophene (BDT), and benzothiadiazole (BT) can be introduced into these bis-DPP compounds. Because they allow for the incorporation of these additional chemical building blocks, bis-DPP compounds are capable of achieving a wider range of structures compared to mono-DPP compounds. Systematic studies of bis-DPP compounds applied as donor materials in organic solar cells are ongoing in our group and will be published elsewhere.

Field Effect Transistors

Conjugated small molecules can also be utilized as the charge transporting layer in FETs. Their p-type or n-type charge transport capabilities can be tuned by modifying their chemical structures and energy levels. Most DPP containing compounds we have investigated have p-type transport characteristics.[23] However, by incorporating electron deficient groups, n-type or ambipolar transport can be achieved. **Figure 5A** shows the chemical structure of a bis-DPP compound (compound 4), which has a BT unit as the central unit flanked with two DPP-T_3C_6 building blocks. Due to the electron deficiency of the BT unit, compound 4 has lower energy levels and is capable of ambipolar transport characteristics.[24] A bottom-gate, top-electrode device structure (**Figure 5B**) was used to measure the ambipolar transport of compound 4. Figures 3C and 3D show the typical transfer characteristics at different annealing temperatures and the corresponding carrier mobilities. Balanced carrier mobilities up to 10^{-3} $cm^2V^{-1}s^{-1}$ were demonstrated using gold electrodes. The electron and hole mobilities can be further improved up to 10^{-2} $cm^2V^{-1}s^{-1}$ by using a low work function electrode such as barium.

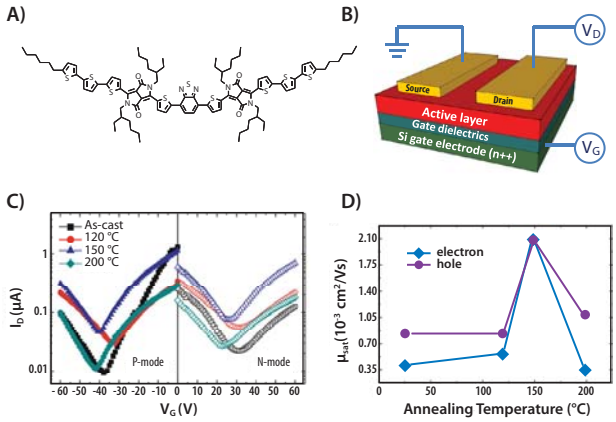

Figure 5. A) Chemical structure of compound 4, capable of ambipolar charge transport. **B)** A schematic illustration of FET device structure. **C)** Saturation transfer characteristics of FETs made from compound 4 at different annealing temperatures using Au top contacts. **D)** Measured carrier mobilities as a function of annealing temperature.[24]

Conclusions

Like their polymeric counterparts, conjugated small molecules have the potential to enable the development of inexpensive, lightweight optoelectronic devices. We briefly summarized several conjugated small molecules containing the DPP chromophore synthesized in our lab for applications in organic solar cells and field effect transistors. Conjugated small molecules allow relatively precise control over material properties such as thermal property, solubility, molecular packing, optical absorption, HOMO and LUMO energy levels, film morphology, and charge transport. This level of materials properties control results from the rational assembly of numerous chemical building blocks such as central chromophores, linkage groups, heteroatom, endcapping groups, and side chains. Using a combination of building block approach and straightforward synthesis, these materials have a vast potential application in optoelectronic devices.

Acknowledgments

We thank ONR and NSF for the financial support and all our collaborators for the contributions to this work.

References

(1) Brédas, J.-L.; Beljonne, D.; Coropceanu, V.; Cornil, J. *Chem. Rev.* **2004**, *104*, 4971.
(2) Boudreault, P.-L. T.; Najari, A.; Leclerc, M. *Chem. Mater.* **2010**, *23*, 456.
(3) Sirringhaus, H.; Kawase, T.; Friend, R. H.; Shimoda, T.; Inbasekaran, M.; Wu, W.; Woo, E. P. *Science* **2000**, *290*, 2123.
(4) Dennler, G.; Scharber, M. C.; Brabec, C. J. *Adv. Mater.* **2009**, *21*, 1323.
(5) He, Z.; Zhong, C.; Huang, X.; Wong, W.; Wu, H.; Chen, L.; Su, S.; Cao, Y. *Adv. Mater.* **2011**, *23*, 4636.
(6) Tsao, H. N.; Cho, D. M.; Park, I.; Hansen, M. R.; Mavrinskiy, A.; Yoon, D. Y.; Graf, R.; Pisula, W.; Spiess, H. W.; Mu¨llen, K. *J. Am. Chem. Soc.* **2011**, *133*, 2605.
(7) Yuen, J. D.; Fan, J.; Seifter, J.; Lim, B.; Hufschmid, R.; Heeger, A. J.; Wudl, F. *J. Am. Chem. Soc.* **2011**, *133*, 20799.
(8) Anthony, J. E. *Chem. Rev.* **2006**, *106*, 5028.
(9) Sun, Y.; Welch, G. C.; Leong, W. L.; Takacs, C. J.; Bazan, G. C.; Heeger, A. J. *Nat Mater* **2012**, *11*, 44.
(10) Walker, B.; Kim, C.; Nguyen, T.-Q. *Chem. Mater.* **2010**, *23*, 470.
(11) Murphy, A. R.; Fréchet, J. M. J. *Chem. Rev.* **2007**, *107*, 1066.
(12) Usta, H.; Facchetti, A.; Marks, T. J. *Acc. Chem. Res.* **2011**, *44*, 501.
(13) Tamayo, A. B.; Tantiwiwat, M.; Walker, B.; Nguyen, T.-Q. *J. Phys. Chem. C* **2008**, *112*, 15543.
(14) Tamayo, A. B.; Dang, X.; Walker, B.; Seo, J. H.; Kent, T.; Nguyen, T. *Appl. Phys. Lett.* **2009**, *94*, 103301.
(15) Walker, B.; Tamayo, A. B.; Dang, X.; Zalar, P.; Seo, J. H.; Garcia, A.; Tantiwiwat, M.; Nguyen, T. *Adv. Funct. Mater.* **2009**, *19*, 3063.
(16) Mei, J.; Graham, K. R.; Stalder, R.; Tiwari, S. P.; Cheun, H.; Shim, J.; Yoshio, M.; Nuckolls, C.; Kippelen, B.; Castellano, R. K.; Reynolds, J. R. *Chem. Mater.* **2011**, 23, 2285.
(17) Lee, O. P.; Yiu, A. T.; Beaujuge, P. M.; Woo, C. H.; Holcombe, T. W.; Millstone, J. E.; Douglas, J. D.; Chen, M. S.; Fréchet, J. M. J. *Advanced Materials* **2011**, 23, 5359.
(18) Loser, S.; Bruns, C. J.; Miyauchi, H.; Ortiz, R. P.; Facchetti, A.; Stupp, S. I.; Marks, T. J. *J. Am. Chem. Soc.* **2011**, 133, 8142.
(19) Sonar, P.; Ng, G.; Lin, T. T.; Dodabalapur, A.; Chen, Z. *J. Mater. Chem.* **2010**, 20, 3632
(20) Walker, B.; Tamayo, A. B.; Duong, D. T.; Dang, X.; Kim, C.; Granstrom, J.; Nguyen, T. Adv. Energy Mater. 2011, 1, 221-229.
(21) Zhang, Y.; Dang, X.; Kim, C.; Nguyen, T. Adv. Energy Mater. 2011, 1, 610-617.
(22) Scharber, M. C.; Mühlbacher, D.; Koppe, M.; Denk, P.; Waldauf, C.; Heeger, A. J.; Brabec, C. J. *Adv. Mater.* **2006**, *18*, 789.
(23) Tantiwiwat, M.; Tamayo, A.; Luu, N.; Dang, X.-D.; Nguyen, T.-Q. *J. Phys. Chem. C* **2008**, *112*, 17402.
(24) Zhang, Y.; Kim, C.; Lin, J.; Nguyen, T. *Adv. Funct. Mater.* **2012**, *22*, 97.

Highly Conductive PEDOT:PSS

Name	Structure	Resistivity	Concentration	Prod. No.
Poly(3,4-ethylenedioxythiophene)-poly(styrenesulfonate) (Orgacon™ S305; PEDOT:PSS)	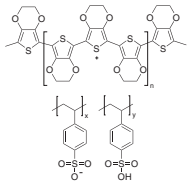	<200 Ω/sq, >90% visible light transmission (40 µm wet)	0.54% in H_2O, (high-conductivity grade)	739340-25G 739340-100G
Poly(3,4-ethylenedioxythiophene)-poly(styrenesulfonate), surfactant-free (Orgacon™ ICP 1050; PEDOT:PSS)		<100 Ω/sq, >80% visible light transmission (40 µm wet)	1.1% in H_2O, (high-conductivity grade)	739332-100G
Poly(3,4-ethylenedioxythiophene)-poly(styrenesulfonate), neutral pH (Orgacon™ N-1005; PEDOT:PSS)		<100 Ω/sq, >70% visible light transmission (40 µm wet)	1.1% in H_2O, (high-conductivity grade)	739324-100G
Poly(3,4-ethylenedioxythiophene)-poly(styrenesulfonate), conductive inkjet ink (Orgacon™ IJ-1005; PEDOT:PSS)		75–120 Ω/sq, >80% visible light transmission (40 µm wet)	0.8% in H_2O	739316-25G

OPV Donor Materials

For a complete list of available products, visit Aldrich.com/oel

Name	Structure	Purity	Properties	Prod. No.
Poly(3,4-ethylenedioxythiophene), bis-poly(ethyleneglycol), lauryl terminated, contains *p*-toluenesulfonate as dopant (Aedotron™ P3-NM; PEDOT:PEG)	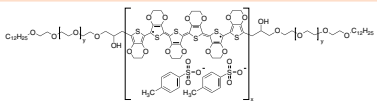	-	0.7 wt. % (dispersion in nitromethane) 0.5-0.9 wt. % (solid concentration)	736295-25G
Poly(3,4-ethylenedioxythiophene), bis-poly(ethyleneglycol), lauryl terminated, contains perchlorate as dopant (Aedotron™ C3-PC, PEDOT)	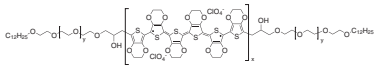	-	0.8 wt. % (dispersion in propylene carbonate)	736287-25G
Polypyrrole-*block*-poly(caprolactone) (Biotron PP-NM; PCL-block-PPy)	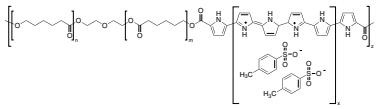	-	0.3-0.7 wt. % (solid) 0.3-0.7 wt. % (dispersion in nitromethane)	735817-25G
Poly(3-hexylthiophene-2,5-diyl), >98% head-to-tail regioregular (HNMR) (P3HT; Plexcore® OS 2100)	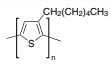	99.995% trace metals basis	electronic grade, average M_n 30,000-60,000	698997-250MG 698997-1G 698997-5G
Poly(3-hexylthiophene-2,5-diyl), >95% head-to-tail regioregular (HNMR) (P3HT; Plexcore® OS 1100)	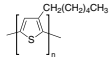	99.995% trace metals basis	electronic grade, average M_n 15,000-45,000	698989-250MG 698989-1G 698989-5G
Poly[(2,5-didecyloxy-1,4-phenylene)(2,4,6-triisopropylphenylborane)], diphenyl terminated (Boramer™-T03, Boramer™-TC03)	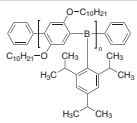	-	average M_n ~1,446	688002-250MG
Poly(3-octylthiophene-2,5-diyl), regioregular (P3OT)	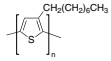	99.995% trace metals basis	electronic grade, average M_n ~25,000	682799-250MG
FTTF	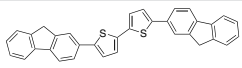	-	-	754056-250MG
SMDPPO	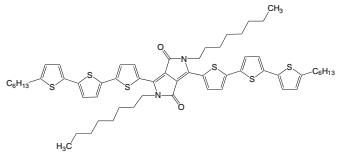	>98%	-	753920-250MG
SMDPPEH	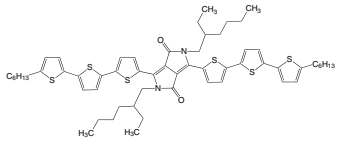	>98%, HPLC	-	753912-250MG
Dithieno[3,2-*b*:2′,3′-*d*]thiophene		97%, HPLC	White to Yellow Powder	710172-500MG

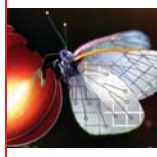

Name	Structure	Purity	Properties	Prod. No.
5,5′-Di(4-biphenylyl)-2,2′-bithiophene	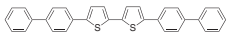	97%	-	695947-1G
5,5‴″-Dihexyl-2,2′:5′,2″:5″,2‴:5‴,2‴″:5‴″,2‴″″-sexithiophene (DH6T)	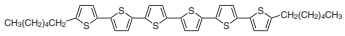	>90%	-	633216-500MG
α-Sexithiophene (Sexithiophene, 6T)	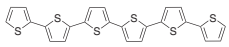	~97%	-	594687-1G
Di-tetrabutylammonium *cis*-bis(isothiocyanato)bis(2,2′-bipyridyl-4,4′-dicarboxylato)ruthenium(II) (N-719 dye) *	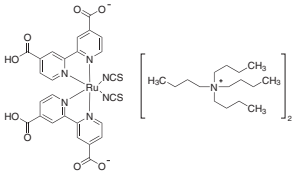	95%, NMR	-	703214-250MG
cis-Bis(isothiocyanato)bis(2,2′-bipyridyl-4,4′-dicarboxylato)ruthenium(II) (N-3 dye) *	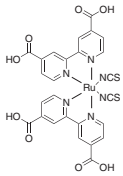	95%, NMR	-	703206-250MG
cis-Bis(isothiocyanato)(2,2′-bipyridyl-4,4′-dicarboxylato)(4,4′-di-nonyl-2′-bipyridyl) ruthenium(II) (Z-907 dye) *	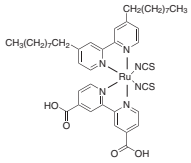	95%, NMR	λ_{max} = 295, 314, 531 nm	703168-250MG

*Dyesol® product

OPV Donor-acceptor Materials

Name	Structure	M_W	Prod. No.
PCBTDPP	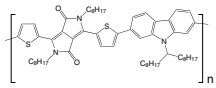	10,000-50,000	754048-100MG
PSiF-DBT	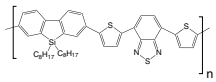	10,000-80,000	754021-100MG
PFO-DBT	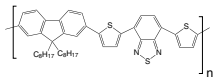	10,000-50,000	754013-100MG
PCPDTBT	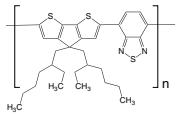	7,000-20,000	754005-100MG
PCDTBT	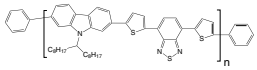	20,000-100,000	753998-100MG

OPV Acceptor Materials

For a complete list of available products, visit Aldrich.com/oel

Name	Structure	Purity	Prod. No.
ICBA	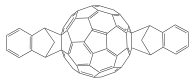	-	753955-250MG
ICMA	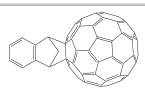	-	753947-250MG

Name	Structure	Purity	Prod. No.
[5,6]-Fullerene-C_{70}		≥99%, HPLC	709476-250MG
C_{60} Pyrrolidine tris-acid	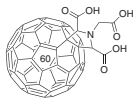	97% (HPLC)	709085-100MG
C_{60} Pyrrolidine tris-acid ethyl ester	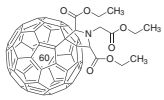	97% (HPLC)	709093-250MG
[6,6]-Phenyl C_{61} butyric acid methyl ester (PCBM)	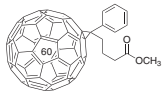	>99%	684430-1G
[6,6]-Thienyl C_{61} butyric acid methyl ester ([60]ThPCBM)	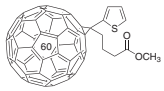	≥99%	688215-100MG
[6,6]-Phenyl-C_{61} butyric acid octyl ester (PCBO)	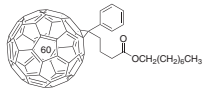	≥99%	684481-100MG
[6,6]-Phenyl-C_{61} butyric acid butyl ester (PCBB)	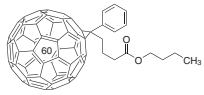	>97%	685321-100MG 685321-1G
[6.6] Diphenyl C_{62} bis(butyric acid methyl ester) (mixture of isomers) (Bis[60]PCBM)	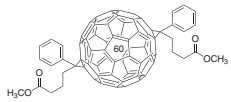	99.5%	704326-100MG
[6,6]-Phenyl C_{61} butyric acid methyl ester (PCBM)	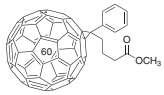	>99.9%	684457-100MG
[6,6]-Phenyl C_{61} butyric acid methyl ester (PCBM)	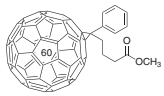	>99.5%	684449-100MG 684449-500MG

Dopants and Conducting Materials

For a complete list of available products, visit Aldrich.com/oel

Name	Structure	Purity	Prod. No.
6,13-Bis((triethylsilyl)ethynyl)pentacene (TES pentacene)	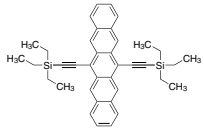	≥99%, HPLC	739278-100MG 739278-500MG
6,13-Bis(triisopropylsilylethynyl)pentacene (TIPS pentacene)	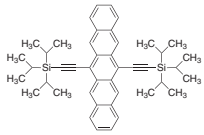	≥99%, HPLC	716006-250MG 716006-1G
Pentacene, triple-sublimed grade	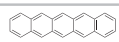	≥99.995% trace metals basis	698423-500MG
Pentacene, sublimed grade	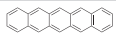	≥99.9% trace metals basis	684848-1G

Name	Structure	Purity	Prod. No.
TES-ADT (5,11-Bis(triethylsilylethynyl)anthradithiophene)	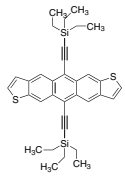	>99%, HPLC	754102-100MG
diF-TES-ADT (2,8-Difluoro-5,11-bis(triethylsilylethynyl)anthradithiophene)	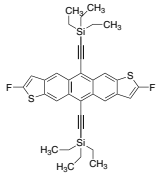	>99%, HPLC	754099-100MG
ADT (Anthra[2,3-*b*:6,7-*b*']dithiophene)	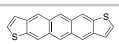	-	754080-250MG
9,10-Bis[(triisopropylsilyl)ethynyl]anthracene (TIPS-anthracene)	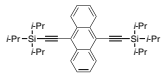	>99%	731439-250MG 731439-1G
Benz[*b*]anthracene, sublimed grade (Tetracene)	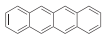	99.99% trace metals basis	698415-1G
1,3,5-Tris(2-thienyl)benzene	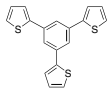	97%	750042-1G
1,3-Dimethyl-2-phenyl-2,3-dihydro-1*H*-benzoimidazole (DMBI)	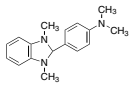	97%	741418-1G
N,*N*'-Di-[(1-naphthyl)-*N*,*N*'-diphenyl]-1,1'-biphenyl)-4,4'-diamine (NPD)	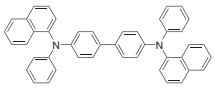	96%	734594-5G
Pentacene-*N*-sulfinyl-*tert*-butylcarbamate	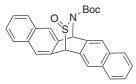	99% (HPLC)	699306-100MG 699306-500MG
N,*N*'-Dipentyl-3,4,9,10-perylenedicarboximide (PTCDI-C5)	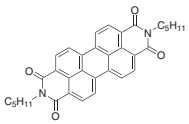	98%	663921-500MG

Organic Conductive Ink Kits

For a complete list of available products, visit Aldrich.com/oel

Name	Application	Prod. No.
Organic conductive inks kit (OC ink system; OC ink kit; Plexcore® OC ink system)	Organic Conductive Inks for printed electronics applications including OLED devices.	719102-1KT
Organic photovoltaic ink system (OPV ink system; Plexcore® PV ink system; Plexcore® PV 1000)	Ready-to-use organic ink system for bulk heterojunction solar cells and spin coating.	711349-1KT

Development of Organic Semiconductors from Highly Ordered Oligo and Polythiophenes



Nicholas S. Colella, Lei Zhang, Alejandro L. Briseño*
Polymer Science & Engineering Department, University of Massachusetts, Amherst, Massachusetts 01003
*Email: abriseno@mail.pse.umass.edu

Introduction

The soaring global demand for energy, coupled with the limited supply of fossil fuels, has increased the need for renewable, low-cost energy sources. Organic electronics have shown great promise for applications in lighting, power, and circuitry, with rapidly improving performance already surpassing that of amorphous silicon-based counterparts.[1,2] Devices designed with organic electronics semiconductors are of relatively low cost because their solution-processable active layers can be printed using traditional textile methods.

The synthesis of new electronically active materials is driving the advances in this burgeoning field. These pi-conjugated systems, including heteroacenes and polythiophenes, are the foundation of organic semiconductor research.[3,4] Thiophenes, oligothiophenes, and polythiophenes have been widely studied in the development of organic electronics; the synthetic accessibility of these molecules and their derivatives have been explored by chemists around the world (**Figure 1**).[5,6] These investigations have led to unprecedented growth in the performance of thiophene-based photovoltaics and organic field-effect transistors (OFETs).[7,8]

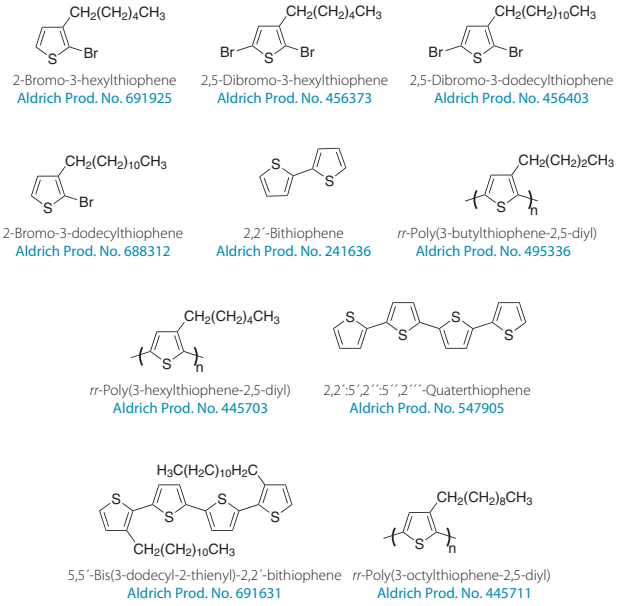

Figure 1. Structures of building blocks, oligothiophenes, and polymer semiconductors.

Synthesis of Oligothiophenes and Polythiophenes

Since substituted polythiophene was first synthesized in 1980, there has been growing interest due to its favorable chemical and physical properties, such as high conductivity, and environmental and thermal stability. However, challenges in processing limited its utility until polythiophenes with flexible side chains were prepared, which improved solubility.[9,10] These early methods carried out solely by chemical and electrochemical strategies produced undesirable head-to-head (HH) and tail-to-tail (TT) couplings, which resulted in a sterically twisted structure in the polymer backbone. This, in turn, affected the thin film microstructure and resulted in poor device performance. In 1992, McCullough et al. developed synthetic methods to afford regioregular Poly(3-alkylthiophene) (rrP3AT) with a HT regioregularity of 98–100%.[11] An alternate route developed by Rieke utilized highly reactive "Rieke® zinc" (ZN*) to prepare regioregular P3ATs. In 1999, the Grignard metathesis (GRIM) method was reported as an economical route to prepare rrP3ATs with the high regioregularity of >99% HT couplings.[11] The GRIM method also offered rapid and easy preparation in large scales under mild reaction conditions. These discoveries brought about not only the development of a wide variety of well-defined polythiophenes, but also a dramatic enhancement in the electrical properties of rrP3ATs, due to planarization of the backbone and solid-state self-assembly to form well-defined, highly organized three-dimensional polycrystalline structures. The synthetic methods are provided in **Scheme 1**. These structures provide efficient intermolecular interactions and supramolecular ordering of the polymer backbone and side chain in the solid state, which lead to high mobility.

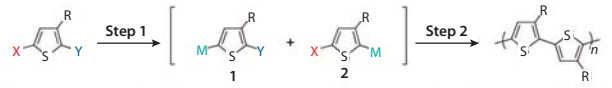

Method	X, Y	Step 1	M (ratio 1:2)	Step 2	HT Regioregularity
McCullough	H, Br	i) LDA/THF, –40 °C, 40 min ii) $MgBR_2 \cdot OEt_2$ ($ZnCl_2$), –60 to –40 °C, 40 min	MgBr (ZnCl) (~98:~2)[a]	$Ni(dppp)Cl_2$, –5 to 25 °C, 18 hr	98–100%
Rieke	Br, Br	Zn*/THF, –78 °C to rt, 4 h	ZnBr (90:10)	$Ni(dppe)Cl_2$, 0 °C to rt, 24 hr	97–100%
GRIM	Br, Br	R′MbX′[b]/THF, rt or reflux, 1 hr	MgX′ (~85:~15)	$Ni(dppp)Cl_2$, rt or reflux, < hr	>99%

a) X for intermediate, **2** is Br (not H) in this case. b) R′ = Alkyl, X′ = Cl, Br

Scheme 1. Synthetic methods for the preparation of regioregular poly(3-alkylthiophene)s.[11] Reprinted with permission from ACS.

Another popular method for producing polythiophenes is via palladium-catalyzed cross-coupling reactions (Stille and Suzuki). By choosing different building blocks, a multitude of molecular architectures have been produced, allowing tuning of the electronic properties over a wide range. However, the Stille and Suzuki polymerization methods have limited control over molecular weight and polydispersity.[11]

In parallel to the remarkable developments surrounding polythiophenes for organic semiconductor materials, oligothiophenes were also realized as promising active semiconductor materials in OFETs. Furthermore, structurally defined, monodisperse oligothiophenes are excellent model compounds for establishing valuable structure-property relationships and extrapolations to their polymer analogs. Although the synthesis of oligothiophenes involves multiple steps, these defect-free materials are

easy to modify by different functional groups, which can provide novel properties to the pi-conjugated core system. Therefore, functionalized oligothiophenes have been considered as a third generation of advanced conjugated materials for organic electronic devices.[7]

Electronic Devices Based on Single Crystals of Oligo- and Polythiophenes

Some of the first devices fabricated from single crystals of a poly(3-hexylthiophene) (P3HT) (Aldrich Prod. Nos. 698989 and 698997) were produced by Cho and coworkers in 2006.[12] They crystallized P3HT from solution onto a self-assembled monolayer (SAM) of silane-treated silicon via a "self-seeding process." This process involved pouring a supersaturated solution of P3HT onto the SAM-modified substrate, resulting in P3HT microwires. Transistors were subsequently fabricated from these microcrystals, using the SAM as a dielectric. The crystal packing showed the 1-D crystal exhibited pi-pi stacking along the long axis with an intermolecular distance of 3.9 Å. Cho and coworkers expanded upon this work by preparing single crystals of P3HT and poly (3-octylthiophene) (P3OT) via solvent vapor annealing and slow, controlled crystallization, respectively.[13] Single crystal transistors with excellent carrier mobilities were reported for both P3HT and P3OT (Aldrich Prod. No. 682799). The results of this study are shown in **Figure 2**.

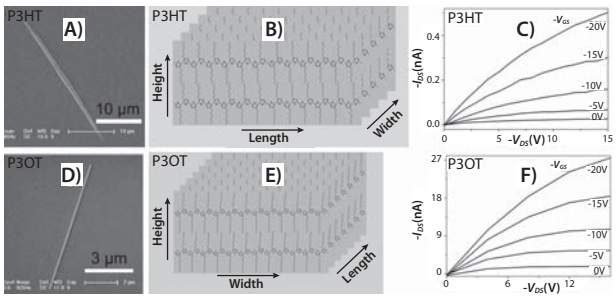

Figure 2. A) TEM image of a P3HT crystal. **B)** Schematic illustration of the crystal structure of P3HT. **C)** Output characteristic of FETs based on a P3HT crystal. **D)** TEM image of a P3OTcrystal. **E)** Schematic illustration of the crystal structure of P3OT. **F)** Output characteristic of FETs based on a P3OT crystal.[13]

Polythiophenes are among the most studied polymers for organic photovoltaics (OPVs). However, they are generally investigated as thin films, where grain boundaries limit their charge transport. The disordered, amorphous regions between crystallites reduce the short-circuit current (J_{sc}) in solar cells, thus limiting their overall efficiency. One common method for overcoming this limited crystallinity is via thermal annealing, which increases the size of the crystallites, thus improving the device performance. Single crystals naturally exhibit better charge transport in OPVs because they do not contain defects which reduce performance. Utilizing this concept, the Jenekhe group designed photovoltaics containing single-crystalline nanowires of poly (3-butylthiophene) (P3BT)[14] (Aldrich Prod. Nos. 495336 and 511420). Nanowires, crystallized by slowly cooling from solution, were mixed with PCBM, a common electron acceptor (**Figure 3**). This mixture was then spin-coated onto indium-tin oxide (ITO) doped glass coated with a hole-conducting layer of PEDOT:PSS. The resulting nanowire network in the active layer of the photovoltaic device was characterized via TEM and AFM, which showed long, thin nanowires with diameters of 8–10 nm and lengths up to 10 μm. Utilizing these materials, solar cells converted light to electrical energy with an efficiency of ~3%, an order of magnitude greater than devices created using polycrystalline thin films of P3BT/PCBM. The nanowires eliminated many trap states in the electron-donating P3BT, lowering the HOMO orbitals, as evidenced by the red-shift in UV-Vis absorption, and slightly increased the open-circuit voltage (V_{oc}). Additionally, the percolating network allowed efficient extraction of charges, resulting in a better fill factor (FF) and increasing the short-circuit current (J_{sc}) by 57%.

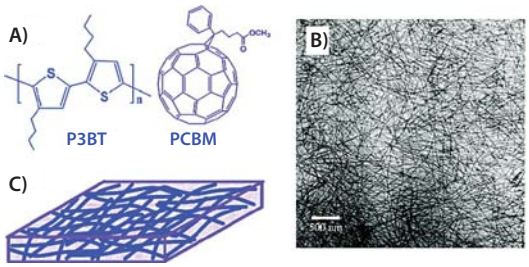

Figure 3. A) Chemical structures of P3BT and C_{61}-PCBM. **B)** TEM images of P3BT-nw/C_{61}-PCBM (1:1 wt% ratio) nanocomposites. **C)** Schematic illustration of nanowire network of P3BT/PCBM composites.

Fundamental research into the crystallization and assembly of organic-inorganic hybrid p-n junctions has also been conducted by Briseno et al. End-functionalized P3HT and dodecyquaterthiophene (QT) were end functionalized with phosphonic acid and subsequently grafted onto zinc oxide (ZnO) nanowires, which resulted in the creation of core-shell p-n junction hybrid nanowires.[15] The crystallographic features of this system were explored via TEM; paralleling their thin-film counterparts, the P3HT shells were less crystalline and exhibited some amorphous domains (**Figure 4**). In contrast, the oligomers self-assembled into single crystals, exhibiting multiple levels of intermolecular interactions, including hydrogen-bonding, van der Waals forces, and pi-pi interactions (**Figure 5**).

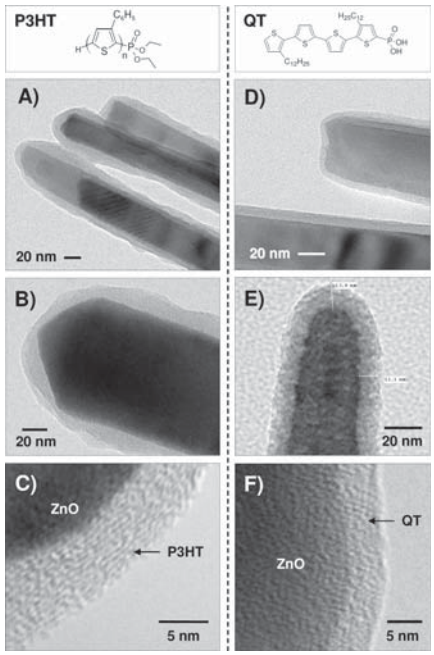

Figure 4. A-C) Transmission electron microscopy (TEM) images of ZnO/P3HT core-shell nanowires and **D-F)** ZnO/QT core-shell nanowires.

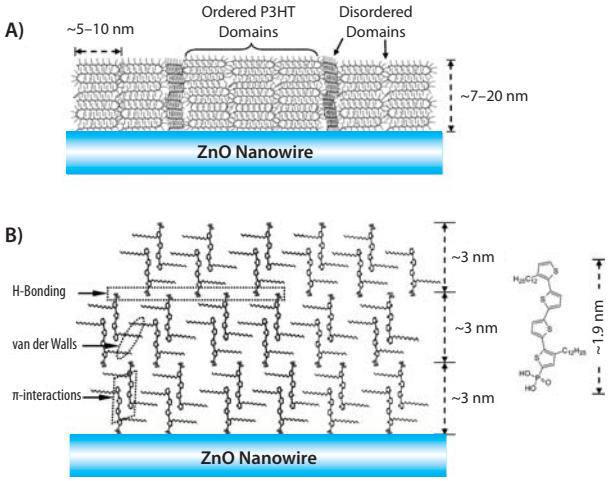

Figure 5. A) Diagram of the ZnO/P3HT interface. **B)** Molecular packing at the ZnO/QT nanowire interface. Also shown are the three molecular forces that drive interfacial self-assembly.

Another demonstration of ordered self-assembly on the nanometer scale was recently presented by Lee et al.[16] In that study, the morphological structure of a polythiophene amphiphilic diblock copolymer which contained nonpolar hexyl and polar triethylene glycol side chains was investigated. While chloroform was a good solvent for both blocks, P3HT crystallized into nanowires upon the addition of a nonsolvent, such as methanol. However, the hydrophilic polythiophene block containing a triethylene glycol side chain was soluble in methanol, and therefore the diblock copolymer formed crystalline aggregates when methanol was added to the chloroform solution. Furthermore, the addition of a salt, such as potassium iodide (KI), drove self-assembly at larger scales in this system. When KI and methanol were added concurrently to a solution of the diblock copolymer in chloroform, superhelical nanowires were observed. Helices resulted from the complexation of the potassium cations by the triethylene glycol side chains (**Figure 6**).

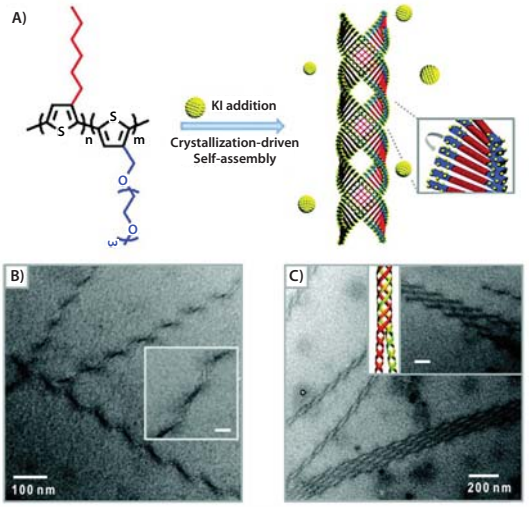

Figure 6. A) Molecular structure of P3HT-*b*-P3(TEG)T diblock copolymers and schematic representation of their assembly into superhelical structures through crystallization in the presence of potassium ions. **B)** TEM images of copolymer after addition of KI revealed helical ribbons with a regular pitch. Inset: magnified image (scale bar: 20 nm). **C)** TEM image of multiple-stranded helices. Inset: TEM image and schematic showing association of double helices into quadruple superhelices (scale bar: 100 nm).

Conclusion

Thiophene-based materials will undoubtedly continue to play a large role in the development of organic electronics. The versatility of these oligomers and polymers will continue to be explored through developments in new synthetic methods and derivatives in order to optimize their molecular, electronic, and morphological properties for increased performance and efficiency. Furthermore, new processing techniques will increase crystallinity, and thus improve performance of the devices based upon these remarkable materials. Single crystals offer the opportunity to study the intrinsic properties of these molecular semiconductors in the solid state and fabricate devices that are not limited in performance by grain boundaries or other morphological defects.

References

(1) Gunes, S.; Neugebauer, H.; Saricitftci, N. S. *Chem. Rev.* **2007**, *107*, 1324.
(2) Murphy, A. R.; Fréchet, J. M. J. *Chem. Rev.* **2007**, *107*, 1066.
(3) Anthony, J. E. *Chem. Rev.* **2006**, *106*, 5028.
(4) Briseno, A. L.; Mannsfeld, S. B. C.; Jenekhe, S. A.; Bao, Z.; Xia, Y. *Mater. Today* **2008**, *11*, 38.
(5) Lim, J. A.; Liu, F.; Ferdous, S.; Muthukumar, M.; Briseno, A. L. *Mater. Today* **2008**, *11*, 38.
(6) Tan, L.; Zhang, L.; Jiang, X.; Yang, X.; Wang, L.; Wang, Z.; Li, L.; Hu, W.; Shuai, Z.; Li, L.; Zhu, D. *Adv. Funct. Mater.* **2009**, *19*, 272.
(7) Mishra, A.; Ma, C.; Bäuerla, P. *Chem. Rev.* **2009**, *109*, 1141.
(8) Zhang, L.; Tan, L.; Wang, Z.; Hu, W.; Zhu, D. *Chem. Mater.* **2009**, *21*, 1993.
(9) Yamamoto, T.; Sanechika, K.; Yamamoto, A. *J. Polym. Sci., Polym. Lett. Ed.* **1980**, *18*, 9.
(10) Sugimoto, R.; Takeda, S.; Gu, H. B.; Yoshino, K. *Chem. Express.* **1986**, *1*, 635.
(11) Osaka, I.; McCullough, R. *Acc. Chem. Res.* **2008**, *41*, 1202.
(12) Kim, D. H.; Han, J. T.; Park, Y. D.; Jang, Y.; Cho, J. H.; Hwang, M.; Cho, K. *Adv. Mater.* **2006**, *18*, 719.
(13) Xiao, X.; Wang, Z.; Hu, Z.; He, T. J. *Phys. Chem. B.* **2010**, *114*, 7452.
(14) Xin, H.; Kim, F. S.; Jenekhe, S. A. *J. Am. Chem. Soc.* **2008**, *130*, 5424.
(15) Briseno, A. L.; Holcombe, T. W.; Boukai, A. I.; Garnett, E. C.; Shelton, S. W.; Fréchet, J. M. J.; Yang, P. *Nano Lett.* **2010**, *10*, 334.
(16) Lee, E.; Hammer, B.; Kim, J.-K.; Page, Z.; Emrick, T.; Hayward, R. C. *J. Am. Chem. Soc.* **2011**, *133*, 10390.

Synthetic Precursors for OPV, OLED, and OFET Materials

For a complete list of available products, visit Aldrich.com/oel

Thiopehene Derivatives

Name	Structure	Purity	Prod. No.
2,5-Dibromo-3,4-dihexylthiophene	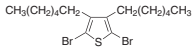	97%	752541-5G 752541-1G
3,4-Dihexylthiophene (3,4-Bis-*n*-hexyl thiophene)	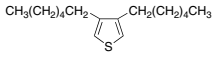	97%	751871-5G
3,3′-Dibromo-5,5′-bis(trimethylsilyl)-2,2′-bithiophene	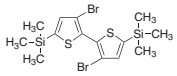	~96% (GC)	751456-1G 751456-5G
5,5′-Bis(trimethylstannyl)-2,2′-bithiophene	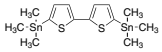	97%	750085-5G 750085-1G
2,5-Bis(trimethylstannyl)-thieno[3,2-*b*]thiophene	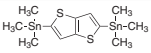	-	741027-1G 741027-5G
5-Bromo-5′-hexyl-2,2′-bithiophene	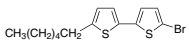	98%	739375-1G 739375-5G
2,5-Bis(trimethylstannyl)thiophene	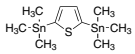	97%	738891-1G 738891-5G
5,5′-Diiodo-2,2′-bithiophene	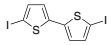	>97%	737429-1G 737429-5G
3,3′,5,5′-Tetrabromo-2,2′-bithiophene	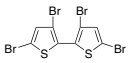	97%	734608-5G
3,3′-Dibromo-2,2′-bithiophene		97%	733725-1G 733725-5G
4,7-Bis(2-bromo-5-thienyl)-2,1,3-benzothiadiazole	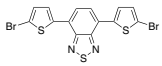	≥99.0%, HPLC	732435-1G
EDOT carboxylic acid	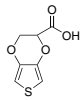	95%	729167-500MG
2-Bromo-3-octylthiophene	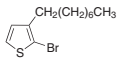	97%	714550-5G
Thieno[3,2-*b*]thiophene		95%	702668-1G 702668-5G
3,3‴-Dihexyl-2,2′:5′,2″:5″,2‴-quaterthiophene (DH-4T)	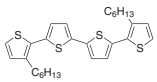	95%	694460-1G
4,7-Dibromobenzo[*c*]-1,2,5-thiadiazole		95%	693847-1G 693847-5G
3,3‴-Didodecyl-2,2′:5′,2″:5″,2‴–quaterthiophene	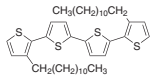	97%	691631-500MG
3,4-Dimethoxythiophene	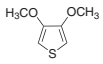	97%	668257-5G

Boronic Acid Derivatives

Name	Structure	Purity	Prod. No.
9-Ethyl-9*H*-carbazole-3-boronic acid pinacol ester	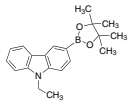	>97%	731757-1G
9-Methyl-9*H*-carbazole-3-boronic acid pinacol ester	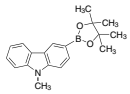	95%	729590-1G
9,9-Dimethylfluorene-2-boronic acid pinacol ester (FL-BE)	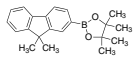	95%	729280-1G
4-(Diphenylamino)phenylboronic acid pinacol ester	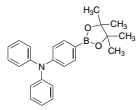	95%	723614-1G 723614-5G
9,10-Anthracenediboronic acid bis(pinacol) ester	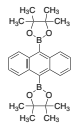	97%	724750-1G
4,4′-Biphenyldiboronic acid bis(neopentyl) ester	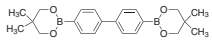	97%	704318-1G
2,1,3-Benzothiadiazole-4,7-bis(boronic acid pinacol ester)	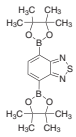	95%	702803-1G

Carbazole and TPA Derivatives

Name	Structure	Purity	Prod. No.
N-(4-Formylphenyl)carbazole	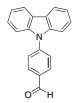	97%	750050-5G
3,6-Dibromo-9-ethylcarbazole	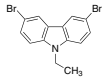	98%	731951-1G
3,6-Dibromo-9-phenylcarbazole	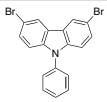	98%	731773-1G
4-Bromo-4′,4″-dimethyltriphenylamine	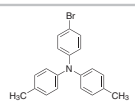	97%	751219-1G 751219-5G
N^1,N^4-Bis(4-butylphenyl)benzene-1,4-diamine	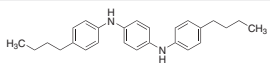	97%	688061-1G
4,4′-Dibromotriphenylamine	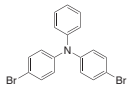	96%	679917-1G 679917-5G
Tris(4-formylphenyl)amine	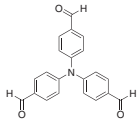	97%	679658-500MG 679658-5G

Precise Nanoparticles for Optoelectronics Applications

Benny Pacheco* and Scott Kordyban**
Product and Business Development Manager
Cytodiagnostics, Inc.
919 Fraser Dr, Unit 11
Burlington, ON L7L 4X8
*Email: bpacheco@cytodiagnostics.com
**Not pictured

Introduction

Inorganic nanomaterials are tunable by size, shape, structure, and/or composition. Advances in the synthesis of well-defined nanomaterials have enabled control over their unique optical, electronic, and chemical properties stimulating tremendous interest across a wide range of disciplines. This article illuminates some of the recent research advances of inorganic nanoparticles (NPs) in optoelectronics applications.

Inorganic Nanostructures and Properties

Since the intrinsic characteristics and relevant applications of nanoparticles are closely related to their size, shape, and surface properties, great efforts have been devoted to the controlled synthesis of nanoparticles. Key properties of nanoparticles (such as gold and silver) can thus be tailored by altering their physical geometries. Numerous publications have addressed the unique properties exhibited by variously metal nanoparticle shapes, including gold nanospheres (**Figure 1**),[1] nanorods,[2] nanoprisms,[3] nanocubes,[4] and nanowires.[5] The optical properties, including optical resonance wavelengths, extinction cross-section, relative contribution of scattering to the extinction, can be tuned for different applications. Spherical nanoparticles offer resonance wavelengths in the visible region, while nanoshell and nanorod resonances are shifted into the Near Infrared (NIR) region. Moreover, nanoshells and nanorods optical properties are enhanced by altering the core-shell radius and aspect ratio, respectively.

Optical properties are conferred by the interaction of light with electrons on the metal nanoparticle surface. At a specific wavelength (frequency) of light, the collective oscillation of electrons on the metal nanoparticle surface causes a phenomenon called surface plasmon resonance, which results in a strong extinction of light. The particular wavelength, or frequency, of light at which this occurs is strongly dependent on the nanoparticle size, shape, surface, and agglomeration state. This strongly enhanced surface plasmon resonance of nanoparticles (especially within the optical frequency range) allows them to be excellent scatterers and absorbers of visible light. This phenomenon, coupled with advances in nanomaterial syntheses,[6] surface conjugation,[7] and self-assembly,[8] has advanced the use of precise plasmon resonant nanostructures for optical,[9] optoelectronics, and biodiagnostic applications.[10]

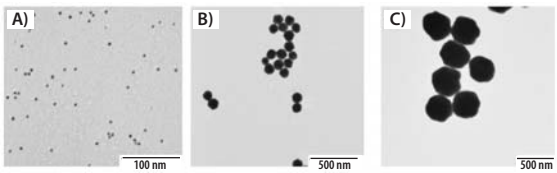

Figure 1. TEM spectra of **A)** 5 nm (Aldrich Prod. No. 741949), **B)** 100 nm (Aldrich Prod. No. 753688), and **C)** 400 nm (Aldrich Prod. No. 742090) gold nanoparticles from Cytodiagnostics and Aldrich Materials Science.

Organic Photovoltaic (OPV) Devices

There have been numerous reports on power conversion efficiency (PCE) enhancement of organic photovoltaic devices using metal nanoparticles. In 2011, an international team of researchers led by Professor Yang at UCLA reported 20% efficiency of existing OPVs using gold nanoparticles (**Figure 2**).[11] They were the first to fabricate a plasmonic-enhanced tandem OPV cell and show the plasmonic effect has future potential for OPV research. In another approach, Chia-Ling Lee and co-workers at the National Chiao Tung University incorporated gold nanoparticles into the anodic buffer layer in an attempt to trigger localized surface plasmon resonance (LSPR) which increased the PCE from 3.57% to 4.2%.[12] It was determined that the improved performance resulted from local enhancement of the electromagnetic field surrounding the gold nanoparticles.

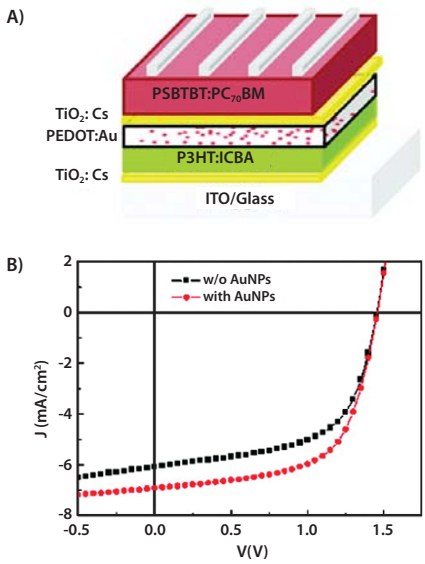

Figure 2. A) Schematic of plasmonic polymer tandem solar cell, ITO/TiO_2:Cs/P3HT:$IC_{60}BA$/PEDOT:Au/TiO_2:Cs/PSBTBT:$PC_{70}BM$/MoO_3/Al. **B)** The J–V characteristics of the tandem solar cells under AM1.5G 100 mW·cm^{-2} illumination.[11] Reprinted with permission from ACS.

Organic Field Effect Transistor (OFET)/ Organic Thin-Film Transistor (OTFT) Materials

The incorporation of inorganic nanoparticles has been investigated in organic thin film transistor (OTFT) devices. Brian Chiang and co-workers at the Xerox Research Center of Canada have solution-deposited metal nanoparticles (primarily gold) to electrodes in a bottom-contact OTFT device using polyquaterthiophene (PQT-12) as an organic semiconductor, as shown in **Figure 3**.[13] The work was carried out at lower temperatures to ensure compatibility with commercially available plastic substrates. The switching capabilities were found to be comparable with analogous devices using more intensive and costly processes such as vacuum deposition of the gold electrodes.

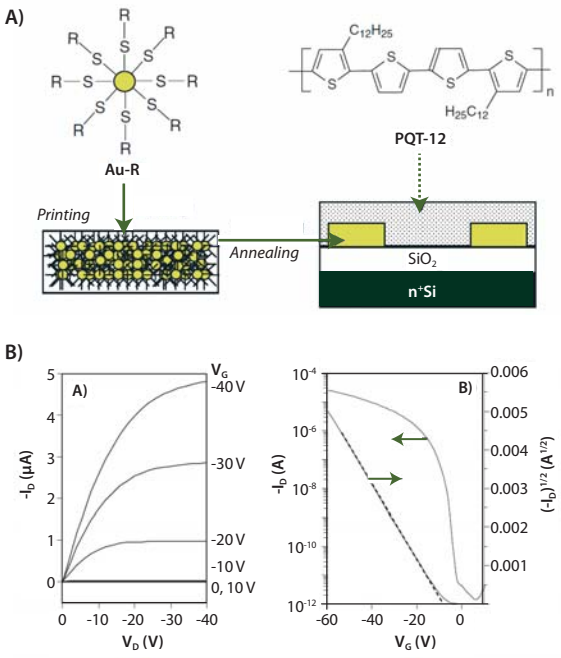

Figure 3. A) Schematic depiction of printing gold source and drain electrodes using gold nanoparticles for a bottom-contact OTFT device using PQT-12 as a semiconductor. **B)** Plot of drain current I_D vs. source-drain voltage V_D as a function of gate voltage V_G for an example OTFT with printed source and drain electrodes with channel length 240 µm and width of 2,200 µm.[13]

Yu-Tai Tao and Chiao-Wei Tseng at the Institute of Chemistry in Taiwan have integrated surface functionalized gold nanoparticles into the conducting channel of a pentacene film-based OFET device.[14] The self-assembly of the gold nanoparticles was shown to dramatically influence the crystallinity and morphology of the thermally evaporated pentacene (Aldrich Prod. No. 698423) films most likely due to the strong metal-pentacene interaction (**Figure 4**). Electric bistability was observed on account of the charge-holding gold nanoparticles; hence, the feasibility of metal nanoparticles to serve as a floating gate in the transistor/ memory function was demonstrated.[14]

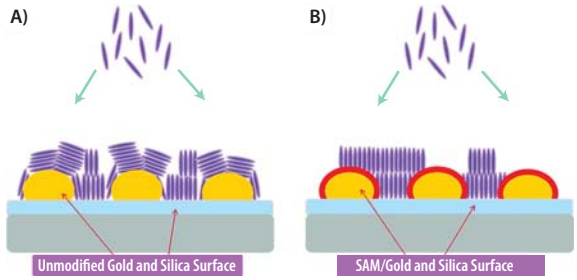

Figure 4. Schematic diagram showing pentacene molecules deposited on silicon substrate decorated with **A)** Unmodified Gold NPs and **B)** SAM-modified Gold NPs.[14] Reprinted with permission from ACS.

Molecular Electronics/Non-Volatile Memory

Srinivasan and co-workers, at the National University in Singapore, have made significant steps toward the enhancement of non-volatile memory and ultimately the realization of nanoparticle-based electronic devices. They have reported the fabrication of a metal-insulator-semiconductor (MIS) device (**Figure 5**) by the covalent attachment of functionalized gold nanoparticles onto a silica substrate using gantrez polymer as a surface modifier.[15] The enhanced stability of the immobilized nanoparticles was tested by sonication. No noticeable change was observed by field emission scanning electron microscopy (FESEM). The MIS device showed well-defined cyclic voltammetry (CV) hysteresis curves, which imply a good memory effect and good retention characteristics up to 20,000 s. Also, the voltage shift was 1.64 V at a swapping voltage of ±7 V.

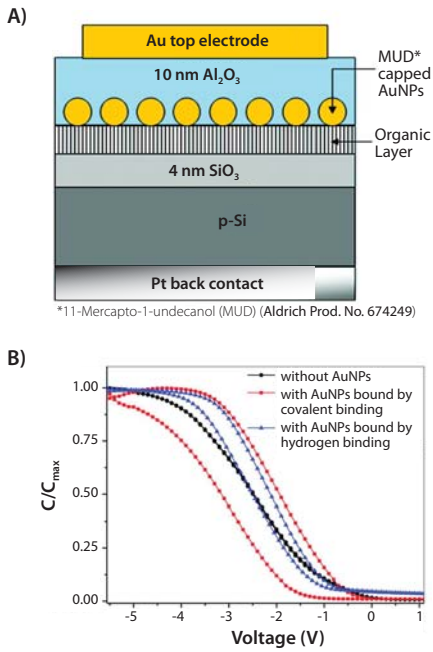

Figure 5. A) MIS device configuration for the immobilized Au nanoparticles. **B)** Normalized *C–V* characteristics at 100 kHz obtained by biasing the top electrodes at ±6 V for control sample (without gold nanoparticle) and with gold nanoparticle.[15] Reprinted with permission from ACS.

Optoelectronics—Fluorescent Nanocrystals

As the world becomes progressively electronic, the efficiency of electronic capture, storage, and presentation of images is continually advancing. As a result, the ability to cost-effectively mass-produce high-performance image sensors and displays is an ongoing challenge. A technology that promises to meet these needs features fluorescent nanocrystals, also known as quantum dots (QDs), which are nanoscale semiconductor crystals, usually held in a liquid suspension. Because of the promise of improved color quality from their light emission, combined with power-efficient operation and cost-effective solution-based processing, fluorescent nanocrystals continue to attract intense academic and commercial interest.

Fluorescent nanocrystals owe their unique light emission and absorption characteristics to their miniature size and quantum confinement. By simply changing the particle size or, in our case the composition, it is possible to tune their bandgaps, emission colors, and absorption spectrum throughout the visible and infrared wavelengths. Because the absorption is broadband, fluorescent nanocrystals are promising for photodetector and photovoltaic applications. Also, their emission is narrow, making them extremely useful materials for displays, lighting applications, optical labeling and barcoding.

Cho et al.[16] have demonstrated a solution-processable active-matrix array (large area) of red light-emitting devices (LEDs) based on CdSe/CdS/ZnS fluorescent nanocrystals (such as those offered by Cytodiagnostics and Aldrich® Materials Science) combined with both organic and inorganic semiconductor layers (**Figure 6**).

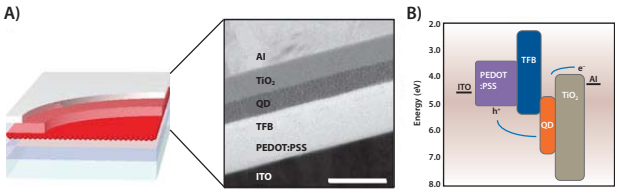

Figure 6. A) Device structure (left) and cross-sectional TEM image (right) of the QD-LED. TFB, poly[(9,9-dioctylfluorenyl-2,7-diyl)-co-(4,4′-(*N*-(4-sec-butylphenyl))diphenylamine)]. Scale bar, 100 nm. **B)** Schematic structure with associated energy band diagram. The QD and TiO_2 energy bands were determined from UPS and optical absorption measurements.[16]

Summary and Future Directions

The symbiosis of organic and inorganic nanomaterials can have some groundbreaking effects on solving some of the research challenges in materials science. Commercially, great care is often taken to ensure in the purity and correct specifications of available organic materials. However, this is not always the case in funcitionalized nanomaterials. Cytodiagnostics and Aldrich® Materials Science are committed to providing customers with products that list the exact specifications and properties of the nanomaterials offered. Highly precise inorganic nanomaterials are becoming an integral part of many research groups worldwide, and as a result we will witness rapid advances in materials science.

References

(1) (a) Link, S.; El-Sayed, M. A. *Int. Rev. Phys. Chem.* **2000**, *19*, 409.
(b) Scaffardi, L. B.; Pellegri, N.; de Sanctis, O.; Tocho, J. O. *Nanotechnology* **2005**, *16*, 158.
(2) (a) Link, S.; El-Sayed, M. A. *J. Phys. Chem. B* **1999**, *103*, 8410.
(b) Sönnichsen, C.; Franzl, T.; Wilk, T.; von Plessen, G.; Feldmann, J.; Wilson, O.; Mulvaney, P. *Phys. Rev. Lett.* **2002**, *88*, 077402.
(3) Millstone, J. E.; Park, S.; Shuford, K. L.; Qin, L.; Schatz, G. C.; Mirkin, C. A. *J. Am. Chem. Soc.* **2005**, *127*, 5312.
(4) Liu, Y.; Walker, A. H. *Angew. Chem. Int. Ed.* **2010**, *49*, 6781.
(5) Graff, A.; Wagner, D.; Ditlbacher, H.; Kreibig, U. *Eur. Phys. J. D* **2005**, *34*, 263.
(6) Burda, C.; Chen, X.; Narayanan, R.; El-Sayed, M. A. *Chem. Rev.* **2005**, *105*, 1025.
(7) Katz, E.; Willner, I. *Angew. Chem., Int. Ed.* **2004**, *43*, 6042.
(8) Mirkin, C. A. *Inorg. Chem.* **2000**, *39*, 2258.
(9) Maier, S. A.; Kik, P. G.; Atwater, H. A.; Meltzer, S.; Harel, E.; Koel, B. E.; Requicha, A. G. *Nat. Mater.* **2003**, *2*, 229-.
(10) (a) Rosi, N. L.; Mirkin, C. A. *Chem. Rev.* **2005**, *105*, 1547.
(b) Chen, J.; Wiley, B. J.; Li, Z.-Y.; Campbell, D.; Saeki, F.; Cang, H.; Leslie, A.; Lee, J.; Li, X.; Xia, Y. *Adv. Mater.* **2005**, *17*, 2255.
(c) Hirsch, L. R.; Stafford, R. J.; Bankson, J. A.; Sershen, S. R.; Rivera, B.; Price, R. E.; Hazle, J. D.; Halas, N. J.; West, J. L. *Proc. Natl. Acad. Sci. U.S.A.* **2003**, *100*, 13549
(d) Chithrani, B. D.; Ghazani, A. A.; Chan, W. C. W. *Nano Lett.* **2006**, *6*, 662.
(e) Loo, C.; Lowery, A.; Halas, N.; West, J.; Drezek, R. *Nano Lett.* **2005**, *5*, 709.
(11) Yang, J.; You, J.; Chen, C.-C.; Hsu, W.-C.; Tan, H.-R.; Zhang, X.; Hong, Z.; Yang, Y. *ACS Nano* **2011**, *5*, 6210.
(12) Chen, F.-C.; Wu, J.-L.; Lee, C.-L.; Hong, Y.; Kuo, C.-H.; Huang, M.; *Appl. Phys. Lett.* **2009**, *96*, 013305.
(13) Wu, Y.; Li, Y.; Ong, B. S.; Liu, P.; Gardner, S.; Chiang, B. *Adv. Mater.* **2005**, *17*, 184.
(14) Tseng, C.-W.; Tao, Y.-T. *J. Am. Chem. Soc.* **2009**, *31*, 12441.
(15) Gupta, R. K.; Kusuma, D. Y.; Lee, P. S.; Srinivasan, M. P. *ACS Appl. Mater. Interfaces* **2011**, ASAP Article.
(16) Cho, K.-S.; Lee, E. K.; Joo, W.-J.; Jang, E.; Kim, T.-H.; Lee, S. J.; Kwon, S.-J. Han, J. Y.; Kim, B.-K.; Choi, B. L.; Kim, J. M. *Nature Photon.* **2009**, *3*, 341.

Nanomaterials

For a complete list of available products, visit Aldrich.com/nanomaterials

Gold Nanoparticles

Name	Formula	Properties	Diameter	Prod. No.
Gold nanoparticles	Au	stabilized suspension in citrate buffer, ~ 5.5E+13 particles/mL	5 nm	741949-25ML 741949-100ML
		stabilized suspension in citrate buffer, ~ 6.0E+12 particles/mL	10 nm	741957-100ML 741957-25ML
		stabilized suspension in citrate buffer, ~ 7.2E+11 particles/mL	20 nm	741965-100ML 741965-25ML
		stabilized suspension in citrate buffer, ~ 1.8E+11 particles/mL	30 nm	741973-100ML 741973-25ML
		stabilized suspension in citrate buffer, ~ 7.2E+10 particles/mL	40 nm	741981-25ML 741981-100ML
		stabilized suspension in citrate buffer, ~ 3.5E+10 particles/mL	50 nm	742007-100ML 742007-25ML
		stabilized suspension in citrate buffer, ~ 1.9E+10 particles/mL	60 nm	742015-25ML 742015-100ML
		stabilized suspension in citrate buffer, ~ 7.8E+9 particles/mL	80 nm	742023-25ML 742023-100ML
		stabilized suspension in citrate buffer, ~ 3.8E+9 particles/mL	100 nm	742031-25ML 742031-100ML
		stabilized suspension in citrate buffer, ~ 1.9E+9 particles/mL	200 nm	742066-25ML 742066-100ML
		stabilized suspension in citrate buffer, ~ 7.1E+8 particles/mL	250 nm	742074-25ML 742074-100ML
		stabilized suspension in citrate buffer, ~ 4.5E+8 particles/mL	300 nm	742082-25ML
		stabilized suspension in citrate buffer, ~ 1.9E+8 particles/mL	400 nm	742090-25ML
		stabilized suspension in citrate buffer, ~ 3.6E+9 particles/mL	150 nm	742058-100ML 742058-25ML
		reactant free; stabilized suspension in 0.1 mM PBS	5 nm	752568-25ML 752568-100ML
		reactant free; stabilized suspension in 0.1 mM PBS	10 nm	752584-25ML 752584-100ML
		stabilized suspension in 0.1 mM PBS, reactant free, ~ 6.5E+11 particles/mL	20 nm	753610-25ML 753610-100ML
		reactant free; stabilized suspension in 0.1 mM PBS	30 nm	753629-25ML 753629-100ML
		stabilized suspension in 0.1 mM PBS, reactant free, ~ 3.5E+10 particles/mL	50 nm	753645-25ML 753645-100ML
		reactant free; stabilized suspension in 0.1 mM PBS	80 nm	753661-25ML 753661-100ML
		reactant free; stabilized suspension in 0.1 mM PBS	100 nm	753688-25ML 753688-100ML
		reactant free; stabilized suspension in 0.1 mM PBS	40 nm	753637-25ML 753637-100ML
		stabilized suspension in 0.1 mM PBS, reactant free, ~ 2.0E+10 particles/mL	60 nm	753653-25ML 753653-100ML

Gold Nanorods

Name	Formula	Properties	Diameter	Prod. No.
Gold nanorods	Au	colloidal suspension; dispersion in H_2O, > 30 µg/mL	10 nm	716812-25ML
		colloidal suspension, > 30 µg/mL 36 µg/mL in H_2O	10 nm	716820-25ML
		colloidal suspension; dispersion in H_2O, > 30 µg/mL	10 nm	716839-25ML
		colloidal suspension; dispersion in H_2O, > 156 µg/mL	25 nm	716847-25ML
		colloidal suspension; dispersion in H_2O, > 211 µg/mL	25 nm	716855-25ML
		colloidal suspension; dispersion in H_2O, > 135 µg/mL	25 nm	716863-25ML
		colloidal suspension; dispersion in H_2O, amine terminated, ≥ 1800.00 µg/mL	10 nm	716871-1ML
		colloidal suspension; dispersion in H_2O, carboxyl terminated, ≥ 1800.0 µg/mL	10 nm	716898-1ML
		colloidal suspension; dispersion in H_2O, methyl terminated, ≥ 1800.0 µg/mL	10 nm	716901-1ML
		colloidal suspension, palladium coated, Au 50 µg/mL in H_2O Pd 38.5 µg/mL in H_2O	25 nm 73 nm (long)	716928-10ML
		colloidal suspension, platinum coated, 100 µg/mL in H_2O	25 nm	716936-10ML
Gold microrods		colloidal suspension dispersion (H_2O), > 50 µg/mL 50 µg/mL in H_2O	200 nm	716960-10ML
Gold nanowires		dispersion (H_2O), > 50 µg/mL 60 µg/mL in H_2O	-	716944-10ML
		dispersion (H_2O), > 50 µg/mL	-	716952-10ML

Silver Nanoparticles

Name	Formula	Properties	Particle Size	Prod. No.
Silver, dispersion (Silverjet DGH-55LT-25C)	Ag	dispersion nanoparticle, for printing on polyimide films, 50-60 wt. % in tetradecane	≤10 nm	736503-25G 736503-100G
		dispersion nanoparticle, for printing on plastic films, 30-35 wt. % in triethylene glycol monomethyl ether	≤50 nm	736465-25G 736465-100G
		nanoparticle, for printing on ITO and glass, 30-35 wt. % in triethylene glycol monoethyl ether	≤50 nm	736481-25G 736481-100G
Silver nanoparticle ink (SunTronic® Silver)		20 wt. % (dispersion in ethanol and ethanediol)	<150 nm (DLS)	719048-5ML 719048-25ML
Silver nanowires		0.5% in isopropanol (suspension)	-	739448-25ML
		liquid (suspension), 0.5% in isopropanol (suspension)	-	739421-25ML
Silver, dispersion		nanoparticle, for printing on ITO and glass, 30-35 wt. % in triethylene glycol monoethyl ether	≤50 nm	736481-25G 736481-100G

Indium Tin Oxide Coated Substrates

Product Description	Surface Resistivity (Ω/sq)	L × W × Thickness (sheet)	Prod. No.
Indium tin oxide coated PET (ITO-PET)	200	1 ft × 1 ft × 5 mil	749745-1EA 749745-5EA
	300	1 ft × 1 ft × 5 mil	749796-5EA 749796-1EA
	250	1 ft × 1 ft × 5 mil	749761-5EA 749761-1EA
	60	1 ft × 1 ft × 7 mil	749729-1EA 749729-5EA
	200	1 ft × 1 ft × 7 mil	749753-5EA 749753-1EA
	250	1 ft × 1 ft × 7 mil	749788-1EA 749788-5EA
	100	1 ft × 1 ft × 7 mil	749737-5EA 749737-1EA
	300	1 ft × 1 ft × 7 mil	749818-1EA 749818-5EA

Metal Oxide Nanoparticles

Name	Formula	Size	Prod. No.
Titanium(IV) oxide (Aeroxide® P25)	TiO_2	nanopowder, particle size ~21 nm	718467-100G
Zinc oxide, dispersion (NanoSunguard™ in water)	ZnO	nanoparticles, avg. part. size <35 nm (APS) particle size <100 nm (DLS)	721077-100G
Zinc oxide, dispersion (NanoSunguard™ in ethanol II)	ZnO	nanoparticles, avg. part. size <35 nm (APS) particle size <130 nm (DLS)	721085-100G
Zinc oxide, dispersion (NanoSunguard™ in butyl acetate)	ZnO	nanoparticles, avg. part. size <35 nm (APS) particle size <110 nm (DLS)	721093-100G
Zinc oxide, dispersion (NanoSunguard™ in butyl glycol)	ZnO	nanoparticles, avg. part. size <35 nm (APS) particle size <120 nm (DLS)	721107-100G

Materials for Self Assembly

For a complete list of available products, visit Aldrich.com/selfassembly

Alkane Thiols

Name	Structure	Purity	Prod. No.
S-(3-Azidopropyl)thioacetate	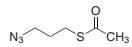	-	752320-1G
1,9-Nonanedithiol	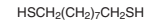	99%	748900-1G
3-Amino-1-propanethiol hydrochloride	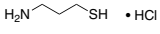	95%	739294-250MG
6-Amino-1-hexanethiol hydrochloride	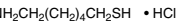	>90%	733679-500MG
[11-(Methylcarbonylthio)undecyl]tri(ethylene glycol) acetic acid	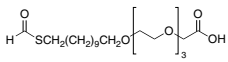	95%	725579-250MG
[11-(Methylcarbonylthio)undecyl]hexa(ethylene glycol) methyl ether	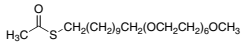	96%	725560-250MG
1,6-Hexanedithiol (DMH)	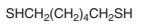	99.5%	725382-1G
12-Mercaptododecanoic acid NHS ester	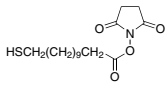	97%	723061-500MG
6-(Ferrocenyl)hexanethiol (FHT)	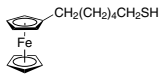	-	682527-250MG
(11-Mercaptoundecyl)hexa(ethylene glycol) (MUHEG)	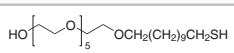	90%	675105-250MG
8-Mercaptooctanoic acid (MOA)	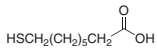	95%	675075-1G
12-Mercaptododecanoic acid (MDA)	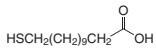	96%	675067-1G
6-Mercaptohexanoic acid (MHA)	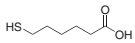	90%	674974-1G
1-Hexadecanethiol n		99%	674516-500MG
(11-Mercaptoundecyl)tetra(ethylene glycol) (MUTEG)	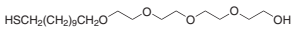	95%	674508-250MG
Bis(10-carboxydecyl)disulfide	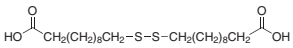	99%	674451-250MG
16-Mercaptohexadecanoic acid (MHDA)	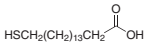	99%	674435-250MG
11-Mercaptoundecanoic acid (MUDA)	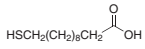	99%	674427-500MG
Dihexadecyl disulfide	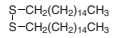	99%	674419-500MG
1,16-Hexadecanedithiol		99%	674400-100MG
11-Amino-1-undecanethiol hydrochloride (MUAM; AUT)	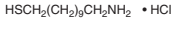	99	674397-50MG
Diundecyl disulfide	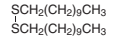	99	674303-250MG
1,11-Undecanedithiol		99%	674281-250MG
1-Nonanethiol		99%	674273-250MG
Bis(11-hydroxyundecyl) disulfide		99%	674257-250MG
11-Mercapto-1-undecanol (MUD)	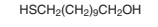	99%	674249-250MG
4-(6-Mercaptohexyloxy)benzyl alcohol	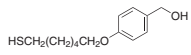	-	673560-50MG
Triethylene glycol mono-11-mercaptoundecyl ether	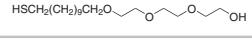	95%	673110-250MG

Name	Structure	Purity	Prod. No.
2-Ethylhexanethiol	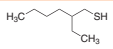	97%	669148-25G 669148-100G
1*H*,1*H*,2*H*,2*H*-Perfluorodecanethiol	$CF_3(CF_2)_7CH_2CH_2SH$	97%	660493-5G 660493-25G
11-Mercaptoundecanoic acid (MUDA)	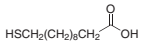	95%	450561-5G 450561-25G
m-Carborane-1-thiol		96%	695572-250MG

Aromatic Thiols

Name	Structure	Purity	Prod. No.
9-Fluorenylmethylthiol FmSH		97%	748889-250MG 748889-1G
9-Mercaptofluorene		97% (GC)	748870-1G
1-Naphthalenethiol		99%	724742-5G
Biphenyl-4,4′-dithiol (BPDT)	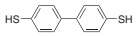	95%	673099-1G

Phosphonic Acids and Silanes

Name	Structure	Purity	Prod. No.
4-Nitrobenzylphosphonic acid	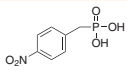	97%	754439-1G
1*H*,1*H*,2*H*,2*H*-Perfluorododecyltrichlorosilane	$CF_3(CF_2)_9CH_2CH_2SiCl_3$	97%	729965-1G 729965-5G
6-Phosphonohexanoic acid (PHA)	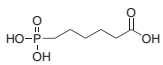	97%	693839-1G
16-Phosphonohexadecanoic acid	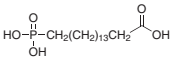	97%	685801-1G
(12-Phosphonododecyl)phosphonic acid	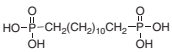	97%	685437-1G
11-Phosphonoundecanoic acid	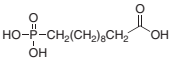	96%	678031-1G
11-Mercaptoundecylphosphoric acid (MDPA)	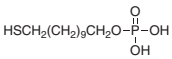	95%	674311-50MG
1*H*,1*H*,2*H*,2*H*-Perfluorooctyltriethoxysilane	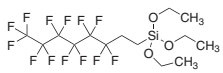	98%	667420-5G 667420-25G

Sigma-Aldrich
3050 Spruce Street
St. Louis, MO 63103 USA

Sigma-Aldrich® Worldwide Offices

Argentina
Free Tel: 0810 888 7446
Tel: (+54) 11 4556 1472
Fax: (+54) 11 4552 1698

Australia
Free Tel: 1800 800 097
Free Fax: 1800 800 096
Tel: (+61) 2 9841 0555
Fax: (+61) 2 9841 0500

Austria
Tel: (+43) 1 605 81 10
Fax: (+43) 1 605 81 20

Belgium
Tel: (+32) 3 899 13 01
Fax: (+32) 3 899 13 11

Brazil
Free Tel: 0800 701 7425
Tel: (+55) 11 3732 3100
Fax: (+55) 11 5522 9895

Canada
Free Tel: 1800 565 1400
Free Fax: 1800 265 3858
Tel: (+1) 905 829 9500
Fax: (+1) 905 829 9292

Chile
Tel: (+56) 2 495 7395
Fax: (+56) 2 495 7396

People's Republic of China
Free Tel: 800 819 3336
Tel: (+86) 21 6141 5566
Fax: (+86) 21 6141 5567

Czech Republic
Tel: (+420) 246 003 200
Fax: (+420) 246 003 291

Denmark
Tel: (+45) 43 56 59 00
Fax: (+45) 43 56 59 05

Finland
Tel: (+358) 9 350 9250
Fax: (+358) 9 350 92555

France
Free Tel: 0800 211 408
Free Fax: 0800 031 052
Tel: (+33) 474 82 28 88
Fax: (+33) 474 95 68 08

Germany
Free Tel: 0800 51 55 000
Free Fax: 0800 64 90 000
Tel: (+49) 89 6513 0
Fax: (+49) 89 6513 1169

Hungary
Tel: (+36) 1 235 9055
Fax: (+36) 1 235 9068

India
Telephone
Bangalore: (+91) 80 6621 9400
New Delhi: (+91) 11 4358 8000
Mumbai: (+91) 22 4087 2364
Pune: (+91) 20 4146 4700
Hyderabad: (+91) 40 3067 7450
Kolkata: (+91) 33 4013 8000
Fax
Bangalore: (+91) 80 6621 9550
New Delhi: (+91) 11 4358 8001
Mumbai: (+91) 22 2579 7589
Pune: (+91) 20 4146 4777
Hyderabad: (+91) 40 3067 7451
Kolkata: (+91) 33 4013 8016

Ireland
Free Tel: 1800 200 888
Free Fax: 1800 600 222
Tel: +353 (0) 402 20370
Fax: + 353 (0) 402 20375

Israel
Free Tel: 1 800 70 2222
Tel: (+972) 8 948 4222
Fax: (+972) 8 948 4200

Italy
Free Tel: 800 827 018
Tel: (+39) 02 3341 7310
Fax: (+39) 02 3801 0737

Japan
Tel: (+81) 3 5796 7300
Fax: (+81) 3 5796 7315

Korea
Free Tel: (+82) 80 023 7111
Free Fax: (+82) 80 023 8111
Tel: (+82) 31 329 9000
Fax: (+82) 31 329 9090

Luxembourg
Tel: (+32) 3 899 1301
Fax: (+32) 3 899 1311

Malaysia
Tel: (+60) 3 5635 3321
Fax: (+60) 3 5635 4116

Mexico
Free Tel: 01 800 007 5300
Free Fax: 01 800 712 9920
Tel: (+52) 722 276 1600
Fax: (+52) 722 276 1601

The Netherlands
Tel: (+31) 78 620 5411
Fax: (+31) 78 620 5421

New Zealand
Free Tel: 0800 936 666
Free Fax: 0800 937 777
Tel: (+61) 2 9841 0555
Fax: (+61) 2 9841 0500

Norway
Tel: (+47) 23 17 60 00
Fax: (+47) 23 17 60 10

Poland
Tel: (+48) 61 829 01 00
Fax: (+48) 61 829 01 20

Portugal
Free Tel: 800 202 180
Free Fax: 800 202 178
Tel: (+351) 21 924 2555
Fax: (+351) 21 924 2610

Russia
Tel: (+7) 495 621 5828
Fax: (+7) 495 621 6037

Singapore
Tel: (+65) 6779 1200
Fax: (+65) 6779 1822

Slovakia
Tel: (+421) 255 571 562
Fax: (+421) 255 571 564

South Africa
Free Tel: 0800 1100 75
Free Fax: 0800 1100 79
Tel: (+27) 11 979 1188
Fax: (+27) 11 979 1119

Spain
Free Tel: 900 101 376
Free Fax: 900 102 028
Tel: (+34) 91 661 99 77
Fax: (+34) 91 661 96 42

Sweden
Tel: (+46) 8 742 4200
Fax: (+46) 8 742 4243

Switzerland
Free Tel: 0800 80 00 80
Free Fax: 0800 80 00 81
Tel: (+41) 81 755 2511
Fax: (+41) 81 756 5449

Thailand
Tel: (+66) 2 126 8141
Fax: (+66) 2 126 8080

United Kingdom
Free Tel: 0800 717 181
Free Fax: 0800 378 785
Tel: (+44) 1747 833 000
Fax: (+44) 1747 833 313

United States
Toll-Free: 800 325 3010
Toll-Free Fax: 800 325 5052
Tel: (+1) 314 771 5765
Fax: (+1) 314 771 5757

Vietnam
Tel: (+84) 8 3516 2810
Fax: (+84) 8 6258 4238

Internet
sigma-aldrich.com

Green U Power

FSC www.fsc.org MIX Paper from responsible sources FSC® C102832

Enabling Science to Improve the Quality of Life

Order/Customer Service (800) 325-3010 • Fax (800) 325-5052
Technical Service (800) 325-5832 • sigma-aldrich.com/techservice
Development/Custom Manufacturing Inquiries SAFC® (800) 244-1173
Safety-related Information sigma-aldrich.com/safetycenter

World Headquarters
3050 Spruce St.
St. Louis, MO 63103
(314) 771-5765
sigma-aldrich.com

OGU
77943-513303
1022